^{208}Pb(d, t) and $(d, {}^3\mathrm{He})$ Reactions with 50-MeV Deuterons*

W. C. PARKINSON,† D. L. HENDRIE, H. H. DUHM,‡ J. MAHONEY, AND J. SAUNDINOS§
Lawrence Radiation Laboratory, University of California, Berkeley, California
AND
G. R. SATCHLER
Oak Ridge National Laboratory, Oak Ridge, Tennessee

(Received 5 August 1968)

The absolute differential cross sections for the six lowest-lying levels of ^{207}Pb and the five lowest-lying levels of ^{207}Tl excited by the ^{208}Pb(d, t) and $(d, {}^3\mathrm{He})$ reactions, respectively, have been measured for 50-MeV incident deuteron energy. In addition, the absolute differential cross sections have been measured for the elastic scattering of 47.5-MeV ^{3}He ions on ^{208}Pb and the inelastic scattering to the well-known 3^- level at 2.615 MeV. The excitation energies and level assignments are in agreement with previous measurements. The measured cross sections, when compared using distorted-wave analysis, suggest that the effective proton shell-model potential may have a larger spatial extent than that for neutrons. In the analysis, the contributions from the nuclear interior to the distorted-wave amplitudes for the proton pickup had to be eliminated, but this was not necessary for the neutron pickup. The distorted-wave analysis is discussed in some detail.

I. INTRODUCTION

IT was suggested by Johnson and Teller[1] some years ago that in spite of the Coulomb repulsion which tends to push the protons to larger radii, the stability against β decay for the heavier nuclei implies a neutron excess on the surface. Since that time some evidence[2] has accumulated that in heavy nuclei the effective radius of the proton distribution is somewhat smaller than that for neutrons and that therefore the nuclear skin is rich in neutrons. A number of experiments have been designed to determine the character of the nuclear surface, and several theoretical discussions on the subject have appeared in print.

Recently an optical-model analysis of 30-MeV proton scattering data by Greenless, Pyle, and Tang[3] led them to conclude in part that the quantity most accurately determined by optical-model analyses of nucleon scattering data is the mean-square radius rather than the shape of the potentials. Using a simple model, they deduce radii for the matter distributions and conclude that the neutron distribution of nuclei extends beyond the proton distribution. (A reassessment[4] of the parameters used in their model indicates, however, that the difference between the two radii may be appreciably less than their analysis implied.) A similar model applied to (p, n) transitions between analog states[5] can also be used to infer that the nuclear surface is neutron-rich.

Two very recent analyses[6] lead to somewhat different conclusions. The energy of the isobaric analog state is used to infer an rms neutron radius for Pb larger than the proton radius by only 0.07 ± 0.03 F, while a reanalysis of 700-MeV pion scattering from Pb suggests that this neutron radius is actually about 2% *smaller* than the proton radius.

If the density distributions for protons and neutrons do have different spatial extents, the effect might be expected to show up in a comparison of neutron and proton pickup reactions, since the important contributions to these are usually confined to the nuclear surface region. The density, however, is an over-all property of *all* the occupied orbitals, whereas in practice pickup experiments only observe the last few occupied orbitals. If the target is a doubly closed shell nucleus like ^{208}Pb, where the lack of fragmentation of the transition strengths indicates that the residual states are quite pure single-particle holes, then the pickup experiment measures the magnitude of the associated single-particle wave function in the surface region. In this way we learn something about the shell-model potential wells which generate these wave functions. We obtain two numbers, the binding energy and pickup strength, for each single-particle state and, if we adopt a specific form for the potential, its optimum parameter values may be determined.

Clearly there is a relation between these neutron

* Research sponsored by the U.S. Atomic Energy Commission under contract with Lawrence Radiation Laboratory, Berkeley, and Oak Ridge National Laboratory.

† Permanent address: The University of Michigan, Ann Arbor, Mich.

‡ Permanent address: Max Planck Institute, Heidelberg, Germany.

§ Permanent address: C.E.N., Saclay, France.

[1] M. H. Johnson and E. Teller, Phys. Rev. **93**, 357 (1954).

[2] A few of the many references are given here; the papers cited list additional references: W. N. Hess and J. Moyer, Phys. Rev. **101**, 337 (1955); S. D. Drell, *ibid.* **100**, 97 (1955); E. H. S. Burhop, Nucl. Phys. **B1**, 438 (1967); L. R. B. Elton, Phys. Rev. **158**, 970 (1967); D. A. Bromley and J. Weneser, Comments Nucl. Particle Phys. **1**, 174 (1967); D. H. Wilkinson, *ibid.* **1**, 80 (1967); E. Rost, Bull. Am. Phys. Soc. **12**, 1193 (1967); a suggestion similar to the last was made in 1955 by L. N. Cooper and W. Tobocman, Phys. Rev. **97**, 243 (1955); see also C. Detrax *et al.*, Phys. Letters **22**, 638 (1966).

[3] G. W. Greenlees, G. J. Pyle, and Y. C. Tang, Phys. Rev. Letters **17**, 33 (1966); Phys. Rev. **171**, 1115 (1968).

[4] D. Slanina and H. McManus, Nucl. Phys. **271**, A1116 (1968).

[5] T. Terasawa and G. R. Satchler, Phys. Letters **7**, 265 (1963); G. R. Satchler, R. M. Drisko, and R. H. Bassel, Phys. Rev. **136**, B637 (1964).

[6] J. A. Nolen, J. P. Schiffer, and N. Williams, Phys. Letters **27B**, 1 (1968); E. H. Auerbach, H. M. Qureshi, and M. M. Sternheim (to be published).

and proton shell model potentials and the neutron and proton density distributions.[3–5] At first sight, a larger radius for the neutron distribution would seem to imply a larger radius for the neutron well. This does not necessarily follow, if only because there are more neutrons than protons. In ^{208}Pb, for example, filling 82 protons and 126 neutrons in wells of the same radius leads to an rms radius for the neutron density which is about 0.3 F larger than for the protons. The analysis of Ref. 3, however, gives 0.64±0.40 F for this difference (see Ref. 4, however), which suggests the neutron potential radius may be larger. This is contrary to what one would expect from optical-model analyses of the elastic scattering of protons. These show an attractive symmetry term, and the interpretation of (p, n) transitions between analog states[5] suggests that this symmetry term is peaked at the surface, at least for some medium-weight nuclei. The implication for the neutron potential is that this term is of opposite sign, repulsive, and (being surface-peaked) equivalent to a *decrease* in radius compared to that for the proton potential. Of course, it may not be valid to extrapolate this expectation to negative energies; the potentials that we are discussing are only the local equivalents to more realistic nonlocal potentials of the Hartree-Fock type.

The (d, t) and $(d, {}^3\mathrm{He})$ reactions on ^{208}Pb are favorable for a study of this kind because of their sensitivity to the radial extent of the bound-state wave functions. For example, a change of 10% in the radius of the Woods-Saxon well typically changes the predicted cross section by about a factor of 2. Any conclusions to be drawn from a comparison of two such measurements, however, imply a good understanding of the reaction mechanism; it is of equal interest, therefore, to assess how well the predictions of the distorted-wave theory describe the data.

II. EXPERIMENTAL

The (d, t) and $(d, {}^3\mathrm{He})$ reactions on ^{208}Pb were studied using 50-MeV deuterons from the Berkeley 88-in. cyclotron. The target was a 1.345-mg/cm^2 self-supporting foil enriched to 99.3% ^{208}Pb. The deuteron beam was energy-analyzed to about 50 keV and brought through the scattering chamber to a split-collector Faraday cup. The currents to the cup halves were used as a beam-centering indicator, and the total current was integrated electronically. The beam spot on the target was approximately 2×4 mm, with an angular divergence of less than 0.3°. Beam currents were varied from a few nA (for small-angle elastic scattering measurements) to the order of 1 μA.

The outgoing particles, ^{3}He or t, were detected in coplanar solid-state detector telescopes mounted in the equatorial plane of the scattering chamber. The telescope for ^{3}He ions consisted of a 0.275-mm phosphorus-diffused silicon ΔE detector and a 3-mm lithium-drifted silicon E detector. For the tritons the ΔE and E counters were 1.5 and 3 mm thick, respectively, and both were lithium-drifted silicon. The triton E detector was rotated 30° from the normal to provide a larger effective thickness. The counter apertures were defined by tantalum collimators at 12.82 and 12.83 in. from the target and subtended solid angles of 1.261×10^{-4} and 1.334×10^{-4}, respectively. The horizontal acceptance angle of each was approximately 0.53°.

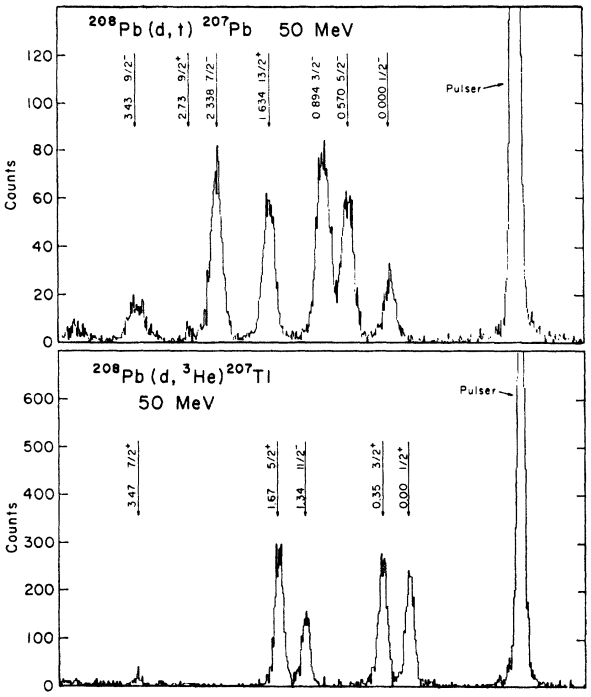

FIG. 1. Sample spectra for the ^{208}Pb(d, t) and $(d, {}^3\mathrm{He})$ reactions. The states discussed are indicated by arrows. The resolution was about 140 keV for the $(d, {}^3\mathrm{He})$ experiment and 180 keV for the (d, t).

The two counter telescopes were rigidly mounted to the same movable arm, with a fixed angle of 21.07° between them. Measurements were made on each side of the incoming beam direction spanning the range from 14° to 82°. In addition to permitting each telescope to move to the same small angles, it also provided a check on the accuracy of the scattering angles and the angular difference of the counters. The efficiency of the counter telescopes was not measured; both were assumed to be 100%. Losses due to inefficiency of the electronics system and reactions occurring in the detectors are not expected to exceed a few percent.

The counter telescopes used for the measurement of the elastic and inelastic scattering of ^{3}He consisted of 0.235- and 0.215-mm ΔE counters and 3-mm E counters. Differential cross sections were measured at a ^{3}He energy of 47.5 MeV from 14° to 136° in the laboratory frame.

Details of the electronics have been described elsewhere and will not be repeated here, other than to note that outgoing-particle types were selected by a

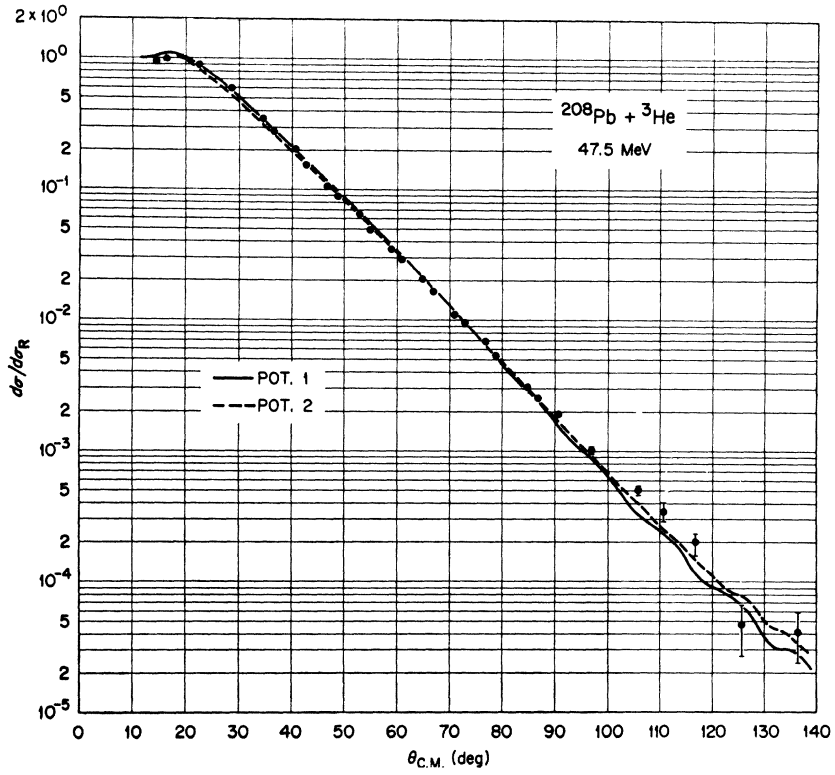

FIG. 2. Differential cross sections for elastic scattering of ^{3}He from ^{208}Pb in ratio to the Rutherford cross sections. The curves are optical-model predictions as described in the text.

Goulding-Landes particle identifier.[7] An important feature was the use of a fourfold-gated pulser of good linearity and accurate timing. Pulses were coupled to the input of each preamplifier throughout the measurements and were recorded with the data. This not only permitted the amplifier gains and the behavior of the particle identification system to be monitored, but, moreover, by observing the loss of coincident pulser pairs between the input and output of the entire electronic system in each telescope, counting losses due to dead times and pile-up were measured. These losses were not permitted to exceed a few percent and chance coincidences between E and ΔE detectors were essentially nil.

The transfer reaction data were taken during two separate runs of 48 h each spaced 10 days in time, while the ^{3}He elastic and inelastic scattering data were taken during one 32-h run a fortnight later. The results of the separate measurements repeated within the statistical expectation.

III. EXPERIMENTAL RESULTS

Examples of the spectra obtained with the ^{3}He and triton counter telescopes and particle-identifier electronics are shown in Fig. 1(a) and 1(b), respectively. The excitation energies of the levels studied and the pulser peak are indicated on each graph. The over-all resolution is about 200 keV, full width at half-maximum (FWHM), which is more than adequate for the investigation of the levels of interest. The lack of appreciable fragmentation of the single-hole states in both ^{207}Pb and ^{207}Tl is evident from the relative simplicity of the spectra.

The measured differential cross sections for the elastic scattering of ^{3}He from ^{208}Pb are shown in Fig. 2 and the differential cross sections for inelastic scattering to the well-known 3^- level at 2.615 MeV are shown in Fig. 3. The fact that data for the 3^- level are a by-product of the elastic scattering measurements accounts for the relatively poor statistics. The measured differential cross sections for six levels observed in the ^{208}Pb(d, t) ^{207}Pb reaction are shown in Fig. 4 and for five levels observed in the ^{208}Pb$(d, ^{3}$He$)$ ^{207}Tl reaction are shown in Fig. 5. The theoretical curves are discussed in Sec. IV. The error bars associated with each datum point reflect the statistical uncertainty in the number of counts and do not reflect possible systematic errors. Systematic errors are expected to be less than 10% of the cross sections. The excitation energies and level assignments for both reactions are in agreement with measurements reported previously.[8,9]

[7] F. S. Goulding, D. A. Landis, J. Cerny, and R. H. Pehl, IEEE Trans. Nucl. Sci. **NS13**, 514 (1966); see also Nucl. Instr. Methods **31**, 1 (1964).

[8] G. Muehllehner, A. S. Poltorak, W. C. Parkinson, and R. H. Bassel, Phys. Rev. **159**, 1039 (1967).

[9] S. Hinds, R. Middleton, J. H. Bjerregaard, O. Hansen, and O. Nathan, Nucl. Phys. **83**, 17 (1966).

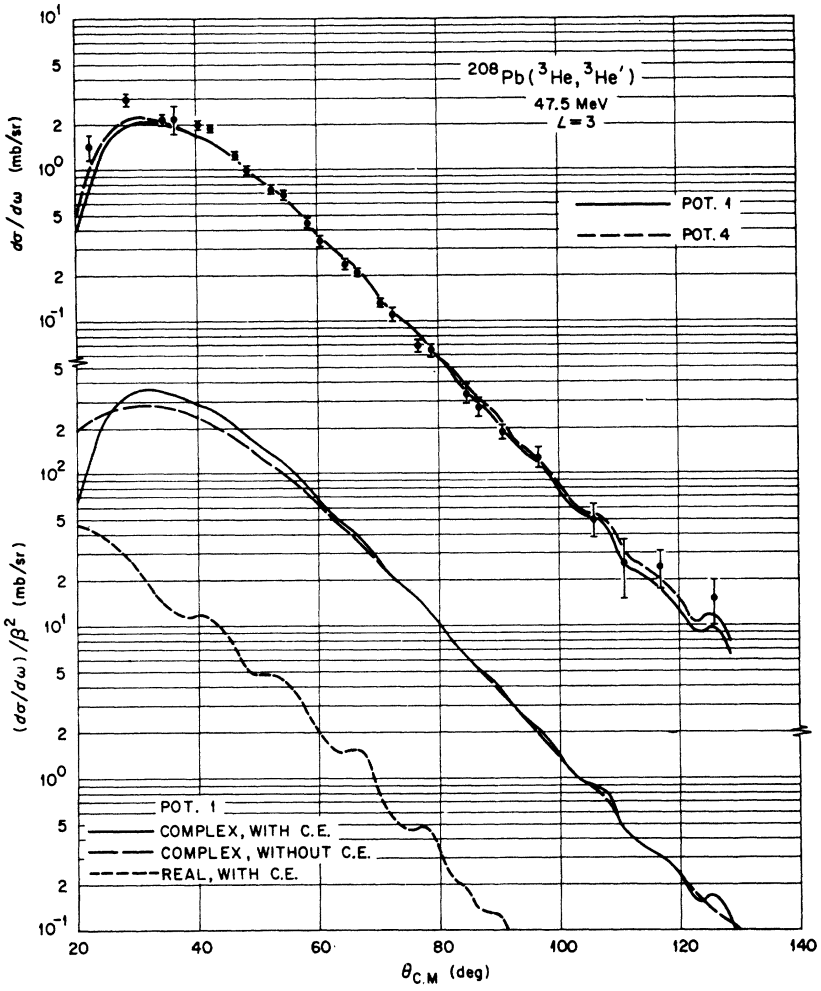

FIG. 3. Differential cross sections for inelastic scattering to the 2.615-MeV 3$^-$ level of ^{208}Pb. The curves are distorted-wave predictions as described in the text. (Note the change of scale for the lower three curves, which are drawn for unit deformation parameter.)

The cross sections for exciting the $\frac{9}{2}^+$ state at 2.73 MeV in ^{207}Pb are very small—no more than 1% of those for the $f_{7/2}$ at 2.34 MeV. There was no evidence of excitation of the 3$^-$ core-excitation doublet expected near 2.6 MeV.

IV. ANALYSIS OF ^{3}He SCATTERING

A conventional analysis of the elastic scattering was made in terms of the optical model, and distorted-wave calculations were made for the inelastic scattering using the collective model.

A. Elastic Scattering

The optical-model potential used has the standard form

$$U(r)=-V(e^x+1)^{-1}-i(W-4W_D d/dx')(e^{x'}+1)^{-1}+(\hbar/m_\pi c)^2 V_s \boldsymbol{\sigma}\cdot\mathbf{L} r^{-1}(d/dr)(e^x+1)^{-1}, \quad (1)$$

where

$$x=(r-r_0A^{1/3})/a, \qquad x'=(r-r_0'A^{1/3})/a'.$$

To this is added the Coulomb potential from a uniformly charged sphere of radius $r_cA^{1/3}$. We took $r_c=1.4$ F, but other values have negligible effects on the results. Except where noted below, the spin-orbit coupling was neglected, $V_s=0$, and, following previous work,[10,11] only volume absorption was considered. That is, we put $W_D=0$.

The parameter values which best fit the data were determined by using an automatic search routine[12] which minimizes the quantity

$$\chi^2=\sum_{i=1}^{N}\left(\frac{\sigma_{\text{theor}}(\theta_i)-\sigma_{\text{expt}}(\theta_i)}{\Delta\sigma_{\text{expt}}(\theta_i)}\right)^2,$$

where $\sigma_{\text{expt}}(\theta_i)$ is the measured, and $\sigma_{\text{theor}}(\theta_i)$ the calculated, differential cross section at angle θ_i, while $\Delta\sigma_{\text{expt}}$

[10] E. F. Gibson, B. W. Ridley, J. J. Kraushaar, M. E. Rickey, and R. H. Bassel, Phys. Rev. **155**, 1194 (1967); C. R. Bingham and M. L. Halbert, *ibid.* **158**, 1085 (1967); B. W. Ridley, T. W. Conlon, and T. H. Braid, Bull. Am. Phys. Soc. **13**, 117 (1967); D. D. Armstrong, A. G. Blair, and R. H. Bassel (to be published).

[11] R. H. Bassel and R. M. Drisko, IPCR Cyclotron Progress Report Suppl. 1, 1968 (unpublished).

[12] R. M. Drisko, The Optical Model Search Code HUNTER (unpublished).

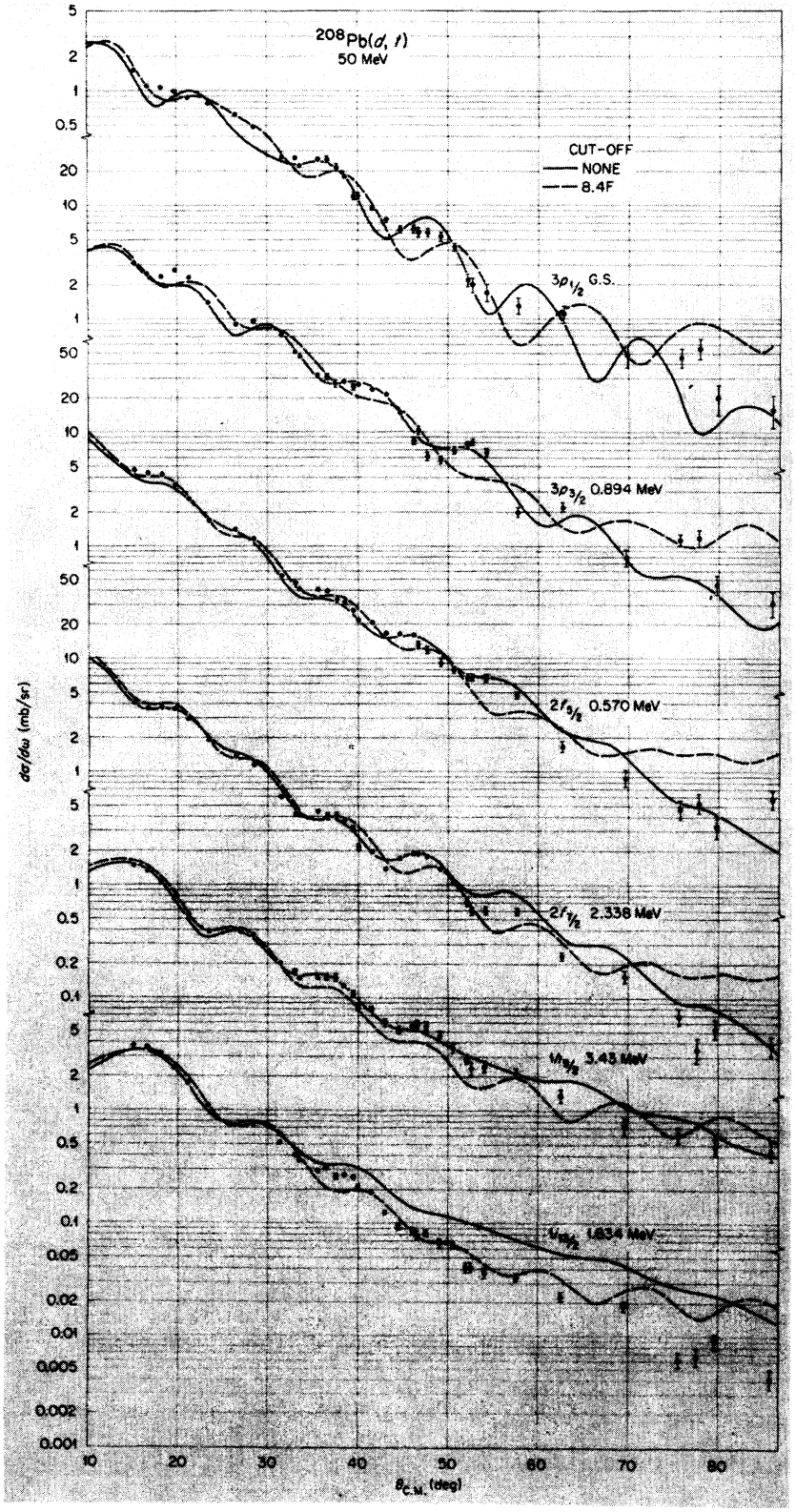

FIG. 4. Differential cross sections for neutron pickup by the ^{208}Pb$(d, t)^{207}$Pb reaction. The excitation energies and angular momenta are given for each group. The curves are distorted-wave predictions as described in the text.

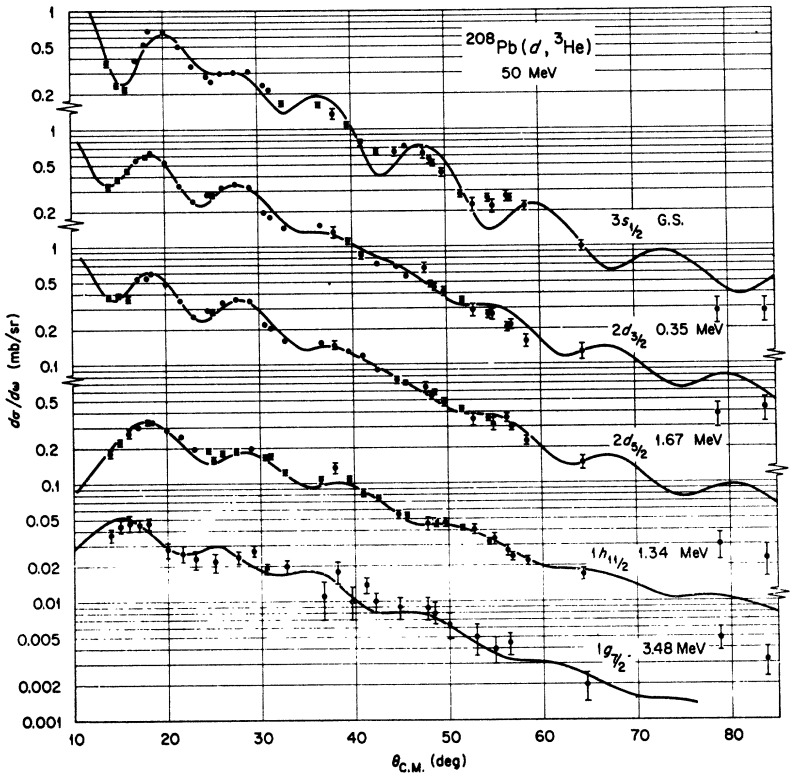

FIG. 5. Differential cross sections for proton pickup by the ^{208}Pb(d, ^{3}He)^{207}Tl reaction. The excitation energies and angular momenta are given for each group. The curves are distorted-wave predictions as described in the text.

is the "error" associated with σ_{expt}. There were $N=29$ data in the present case. Use of the experimental errors for $\Delta\sigma_{expt}$ gave entirely too much weight to the most forward angles, while uniform weighting, $\Delta\sigma_{expt}=$ const, gave undue importance to the large angles. Preliminary calculations indicated that a reasonable choice was $\Delta\sigma_{expt}/\sigma_{expt}=10\%$ for the first 23 angles and 50% for the remaining six.

Previous studies[10,11] have shown that the scattering from lighter nuclei can be well described by a potential with "geometrical" parameters $r_0=1.14$ F, $a=0.723$ F, $r_0'=1.6$ F, and $a'=0.81$ F, with optimum well depths close to $V=175$ MeV and $W=17.5$ MeV. There are considerable ambiguities in the choice of an optical potential for ^{3}He scattering, but potentials of the type just described have been found to give good results when used in distorted-wave calculations of transfer reactions.[11] We note that the real well is roughly three times as strong as that for a single nucleon.

The initial studies of the present data showed that the ambiguities are even more severe than usual. This is not entirely unexpected; a glance at Fig. 2 shows that the angular distribution is very structureless and in ratio to the Rutherford cross section it is simply exponential. This implies that we cannot hope to determine with any precision the values of all six parameters. In addition, past experience shows that the scattering is much less sensitive to variations in the parameters of the real part of the potential than to those in the imaginary part. For these reasons, most of the present studies were made with the fixed values $r_0=1.14$ F and $a=0.723$ F, and many with the well depth fixed at $V=175$ MeV also.

The imaginary potential parameters $r_0'=1.6$ F and $a'=0.81$ F, with $W\approx17.5$ MeV, found suitable for lighter nuclei,[10] yield for Pb an angular distribution which is structureless but does not fall off fast enough with increasing angle. Varying V and W alone leads to little change in V, but to a reduction in W to about 12 MeV; however, this introduces marked oscillations into the angular distribution. These oscillations are removed by allowing r_0' and a' to vary also; the optimum values are included in Table I as potential 4. No significant reduction in χ^2 is obtained by then allowing the values of r_0 and a to vary also (potential 5).

When distorted-wave calculations of the (^{3}He, d) reaction were made with this potential 4, it was found to be objectionable in the sense that it gives such strong absorption for the ^{3}He, and hence results in small transfer cross sections, that the spectroscopic factors needed to reproduce the observed cross sections were very much larger than anticipated. Since it was suspected that this strong absorption was unrealistic, more restricted optical-model searches were made. The values of $V=175$ and $W=17.5$ were fixed, and either r_0' or a' was optimized independently. Varying r_0' alone

TABLE I. Optical-potential parameters for ^{3}He scattering from ^{208}Pb at 47.5 MeV.

Potential	V (MeV)	r_0 (F)	a (F)	W (MeV)	r_0' (F)	a' (F)	σ_A (mb)	χ^2
1	175.0	1.14	0.723	17.5	1.6	0.901	2658	18
2	175.0	1.14	0.723	23.3	1.6	0.927	2873	13
3	159.9	1.14	0.723	22.3	1.6	0.927	2844	13
4	156.1	1.14	0.723	26.4	1.534	0.970	2813	12
5	155.9	1.202	0.631	27.7	1.508	1.009	2827	11

increased its value above 1.6 F, and produced some improvement in fit, but most improvement was obtained by simply increasing a' to about 0.9 F. The scattering predicted by this (potential 1 of Table I) is compared with the data in Fig. 2 (solid curve). Allowing W to vary also (potential 2) gives some reduction in χ^2; as shown in Fig. 2 (dashed curve), this comes mostly from large scattering angles. It is not obvious that this represents any real improvement, since the fit is actually worsened a little at the forward angles. Changes in the value of V (potential 3) produce no significant change in χ^2.

The predicted absorption cross sections σ_A (Table I) show the varying degrees of absorption due to these potentials. The potential obtained from lighter nuclei with $a'=0.81$ F gives $\sigma_A=2481$ mb, and the increase to $a'=0.9$ F in potential 1 leads to 2658 mb. Variation of more parameters leads to even larger values of over 2800 mb. These changes are shown in the reflection coefficients η_L. These show the usual strong absorption behavior that $|\eta_L|$ is very small for small L, rising rapidly to unity at the L value corresponding to a glancing collision. This critical L value is approximately one unit larger for potential 4 than for potential 1.

It is clear from Fig. 2 that the measured cross sections at 14° and 16° are low by about 10%; the theoretical predictions at these angles are very stable. For this reason, the effect of renormalizing the measured cross sections by 1.1 was studied. When the parameters were constrained as for potential 1, there was little change; the optimum $a'=0.877$ F with $\chi^2=12$. Varying other parameters, however, generally led to less strongly absorbing potentials than those given in Table I. Although the minimum χ^2 values tended to be smaller than those obtained with the original data, in no case was the improvement large enough to be considered very significant.

The effect of including some spin-orbit coupling was found to be very small. For example, adding a spin-orbit term with $V_s=3$ MeV to potential 1 produced changes of at most a few percent, and those were at large angles. Further, the polarizations predicted are very small, being everywhere less than 10%.

To summarize, we believe that the only significant result from this analysis is that an increase in a' is required, compared to lighter nuclei, to give the observed rate of fall with angle. An acceptable fit to the measured cross sections is obtained this way and to some extent, at least, the variations in the other parameters are not very meaningful. For this reason, we shall adopt potential 1 for the distorted-wave calculations of the transfer reactions to be described later. There is evidence[13] that the imaginary potential for ^{3}He depends upon the asymmetry parameter $\epsilon=(N-Z)/A$, and that this is a surface effect. The current interpretation of this effect is equivalent to having r_0' increase as ϵ increases. However, in the present case there seems to be a definite preference for an increase in the diffuseness a' rather than the radius. It would be interesting to have scattering data for Pb at higher energies where the angular distributions would exhibit more structure and allow the parameters to be determined more easily.

B. Inelastic Scattering

Distorted-wave calculations were made for the excitation of the 3^- state at 2.615 MeV. The collective-model interaction[14] was used, which treats this level as an octupole vibration and assumes that the optical potential undergoes the same oscillations in shape. It was early noted[15] that a consistent description of ^{3}He inelastic scattering requires one to deform both the real and imaginary parts of the potential. Indeed, because it extends to larger radii the imaginary part gives the majority of the cross section.

Calculations were made with potentials 1 and 4. Contributions from Coulomb excitation were included by assuming a uniformly charged sphere of radius 1.2 $A^{1/3}$ vibrating with the same deformation parameter as the optical potential.[14] The upper part of Fig. 3 compares the results with the measured cross sections; deformation parameters of $\beta_3=0.076$ (potential 1) and 0.080 (potential 4) were used in drawing the theoretical curves. Similar analyses of the excitation of this level

[13] R. M. Drisko, P. G. Roos, and R. H. Bassel, J. Phys. Soc. Japan Suppl. **24**, 347 (1968).
[14] R. H. Bassel, R. M. Drisko, G. R. Satchler, and E. Rost, Phys. Rev. **128**, 2693 (1962).
[15] E. R. Flynn and R. H. Bassel, Phys. Rev. Letters **15**, 168 (1965); E. F. Gibson, J. J. Kraushaar, B. W. Ridley, M. E. Rickey, and R. H. Bassel, Phys. Rev. **155**, 1208 (1967); C. R. Bingham and M. L. Halbert, *ibid.* **158**, 1085 (1967).

by neutrons,[16] protons,[17] and α's[18] have led to deformation parameters $\beta_3=0.12\pm0.01$, which are significantly larger than those found here. However, the values of $\beta_3 R$ (where R is the nuclear radius) for the various experiments are much closer[19] if we use for R in the present case the radius of the *imaginary* part of the optical potential.

The lower part of Fig. 3 shows theoretical curves for potential 1 drawn for unit deformation (the cross sections being proportional to β_3^2). Including the Coulomb excitation produces small but noticeable changes in the predicted cross sections. This figure also emphasizes that deforming only the real part of the potential would give cross sections which are an order of magnitude smaller (and hence lead to deformation parameters correspondingly larger, $\beta_3\approx0.4$). It also gives more structure in the predicted angular distribution than is seen experimentally.

When the imaginary part of the optical potential is also deformed, the resulting amplitude overwhelms the other contributions.

It is interesting that both optical potentials (and others that were also tried) predict very similar inelastic cross sections, so that the potential ambiguity for the elastic scattering carries over into the inelastic transitions also when the collective model is used.

V. DISTORTED-WAVE THEORY OF TRANSFER REACTIONS

A. Distorted-Wave Method

Distorted-wave calculations of the conventional type were made using the computer code JULIE.[20] Application of the theory to the pickup reactions $(d, {}^3\mathrm{He})$ and (d, t) has been discussed elsewhere,[21] but we must draw attention here to some specific points. The zero-range approximation was used, with the normalization due to Bassel,[22] namely, $D_0^2(d, {}^3\mathrm{He})=2.99\times10^4$ MeV^2 F^3, and $D_0^2(d, t)=3.37\times10^4$ MeV^2 F^3. Finite-range corrections may be easily included by use of the local-energy approximation,[21] but these corrections are small with the optical potentials used here. In view of the further uncertainties to be discussed below, they were not included in the results to be described here except when otherwise stated.

B. Spin-Orbit Coupling

There is definite evidence for the need for a spin-orbit coupling term in the deuteron optical-model potential,[23,24] and it is reasonable to suppose there is a similar interaction term for the mass-3 particles. However, the large number of partial waves required to describe the reactions and the limitations of the presently available code excluded calculations including spin-orbit distortions for angular momentum transfers greater than $d_{5/2}$. Fortunately, it appeared that the spin-orbit effects were negligible for all except the (d, t) transitions with $l=1$. The effects of spin-orbit coupling on the wave function of the captured nucleon are important, however, and were always included.

C. Optical-Potential Uncertainties and Nonlocality

The optical-model parameters are obtained, in principle, by the analysis of the appropriate elastic scattering data. In practice, as we have already seen for the ^{3}He scattering, there remain ambiguities and uncertainties in these parameter values. The determination of the deuteron and triton potentials is discussed below. It will be seen that we have followed the prescription that has been found most successful previously; namely, the deuteron potential has a strength roughly twice that for a single nucleon, while the potential for mass 3 is about three times the strength. (This combination also minimizes the finite-range corrections.[21]) Further, the elastic scattering observations only determine the asymptotic form of the distorted waves (namely, that "outside" the nucleus) and it is a major extrapolation to use the simple optical-model wave functions in the nuclear interior. One feature usually neglected in the phenomenological optical model is the nonlocality of the "true" optical potential. The local phenomenological potentials used are assumed to be equivalent in the sense that they yield the same scattering. However, the corresponding wave functions will differ in the nuclear interior; in particular, the distorted wave generated by the nonlocal potential is reduced in the interior compared to that from the equivalent local potential.[25] This reduction can be easily and accurately computed for one kind of nonlocality that is often

---

[16] L. Cranberg, in *Progress in Fast Neutron Physics*, edited by G. C. Phillips, J. B. Marion, and J. R. Risser (University of Chicago Press, Chicago, Ill., 1963); P. H. Stelson, R. L. Robinson, H. J. Kim, J. Rapaport, and G. R. Satchler, Nucl. Phys. **68**, 97 (1965).

[17] M. P. Fricke and G. R. Satchler, Phys. Rev. **139**, B567 (1965).

[18] G. R. Satchler, H. W. Broek, and J. L. Yntema, Phys. Letters **16**, 52 (1965).

[19] J. S. Blair, in *Proceedings of the Conference on Direct Interactions and Nuclear Reaction Mechanisms, Padua*, 1962, edited by E. Clementel and C. Villi (Gordon and Breach, Science Publishers, Inc., New York, 1963).

[20] R. H. Bassel, R. M. Drisko, and G. R. Satchler, Oak Ridge National Laboratory Report No. ORNL-3240 and Supplement (1962) (unpublished).

[21] J. C. Hiebert, E. Newman, and R. H. Bassel, Phys. Rev. **154**, 898 (1967).

[22] R. H. Bassel, Phys. Rev. **149**, 791 (1966).

[23] J. Raynal, Phys. Letters **7**, 281 (1963); C. M. Perey and F. G. Perey, Phys. Rev. **152**, 923 (1966).

[24] F. Hintenberger, G. Mairle, U. Schmidt-Rohr, G. J. Wagner, and P. Turek, Nucl. Phys. **A111**, 265 (1968).

[25] N. Austern, Phys. Rev. **137**, B752 (1965); F. G. Perey, in *Proceedings of the Conference on Direct Interactions and Nuclear Reaction Mechanisms, Padua*, 1962, edited by E. Clementel and C. Villi (Gordon and Breach, Science Publishers, Inc., New York, 1963).

TABLE II. Optical-potential parameters used for distorted-wave calculations of nucleon transfer.

Particle	V (MeV)	r_0 (F)	a (F)	W (MeV)	W_D (MeV)	r_0' (F)	a' (F)	r_c (F)	V_s (MeV)
d	91	1.16	0.83	0	14.25	1.25	0.90	1.3	6[a]
^{3}He	175	1.14	0.723	17.5	0	1.60	0.90	1.4	3[a]
t	160	1.14	0.723	17.5	0	1.50	0.90	1.4	3[a]
p	V_p	1.25	0.63	...	...	...	...	1.25	$\lambda_p=15$[b]
n	V_n	1.25	0.63	...	...	...	...	...	$\lambda_n=27.5$[b]

[a] Set equal to zero except when specified in the text.
[b] Spin-orbit coupling of λ times the Thomas term used; corresponds to $V_{sp}\approx 5$ MeV, $V_{sn}\approx 7$ MeV.

postulated[26] by using the so-called local-energy approximation. This yields a damping factor

$$D(r)=C[1-(\mu\beta^2/2\hbar^2)\,U(r)]^{-1/2}, \qquad (2)$$

where μ is the reduced mass of the projectile, β is the range of nonlocality,[26] and $U(r)$ is the equivalent local potential. [In the applications to be described, only the real part of $U(r)$ is used.] The constant C is unity for scattering states, but greater than unity for bound states in order to conserve normalization. (Typically, $C\approx 1.15$–1.20 for a bound nucleon if $\beta\approx 0.85$ F.) The observed energy dependence of the local potentials implies that $\beta\approx 0.85$ F for nucleons, $\beta\approx 0.54$ F for deuterons, and $\beta\sim 0.3$ F for ^{3}He. Since three factors (2) enter the distorted-wave matrix element, appreciable reductions of the interior contributions may result.

However, other kinds of nonlocality are possible and likely, and may lead to greater reductions in the wave functions in the nuclear interior.[27] If these are indeed present, they could explain why one sometimes obtains better fits to the measured stripping angular distributions when the contributions from the interior are completely removed by using a sharp cutoff on the stripping radial integrals. Possible evidence of a need for increased damping of this kind has been found for both (d, p) and (p, d) reactions.[28] We do not have any simple prescription like Eq. (2) for more general types of nonlocality. The use of a *sharp* radial cutoff is objectionable; however, a rounded damping factor like Eq. (2) would involve three parameters (a strength, radius, and surface thickness). It is not unreasonable, perhaps, to use the form of Eq. (2), with increased β values but the other parameters determined by the optical potentials, as a purely phenomenological device. Some studies in this direction are reported below.

[26] W. E. Frahn and R. H. Lemmer, Nuovo Cimento **6**, 664 (1957); F. G. Perey and B. Buck, Nucl. Phys. **66**, 358 (1965).
[27] R. E. Schenter, Nucl. Phys. **A94**, 408 (1967); G. H. Rawitscher, Phys. Rev. **163**, 1223 (1967).
[28] J. L. Yntema and H. Ohnuma, Phys. Rev. Letters **19**, 1314 (1967); J. Philpott, W. T. Pinkston, and G. R. Satchler, Nucl. Phys. **A119**, 241 (1968).

D. Deuteron Optical Potential

This was obtained by fitting the 52-MeV cross-section data taken at the Karlsruhe cyclotron,[24] using an optical potential of the form (1) with surface absorption ($W=0$). A vector spin-orbit coupling term was included; for this, the operator $\boldsymbol{\sigma}$ in Eq. (1) was interpreted as the operator appropriate for spin 1. The optimum parameters are listed in Table II; the corresponding absorption or reaction cross section is predicted to be 2932 mb. The theoretical and experimental cross sections are compared in Fig. 6. Searches were also conducted omitting the spin-orbit term ($V_s=0$), but this results in much deeper minima in the angular distributions which cannot be removed by adjusting the other parameters. The spin-orbit term appears to be essential, as has been noted before.[23,24] Further, it appears to be necessary to have a real well depth of $V\sim 100$ MeV (i.e., about twice the depth of a typical nucleon optical potential).

Additional reductions in χ^2 were obtained by allowing both volume and surface absorption terms. An optimum volume imaginary term with $W\approx 3.4$ MeV was found, with a corresponding reduction in W_D and small readjustments in the other parameters. However, the improvement in fit was not very great and is not expected to make any noticeable changes in the distorted-wave calculations. For these latter, the potential in Table II was used.

E. Triton Optical Potential

The elastic scattering of tritons from nuclei in the region of Pb has not been measured at energies (45–49 MeV) appropriate to the (d, t) measurements discussed here. In order to determine the triton parameters for the distorted-wave calculations we are forced to extrapolate from much lighter nuclei ($A\lesssim 100$) and lower energies[29] ($E\lesssim 20$ MeV). We choose to do this in terms of the symmetry relation between triton and ^{3}He po-

[29] J. C. Hafele, E. R. Flynn, and A. G. Blair, Phys. Rev. **155**, 1238 (1967).

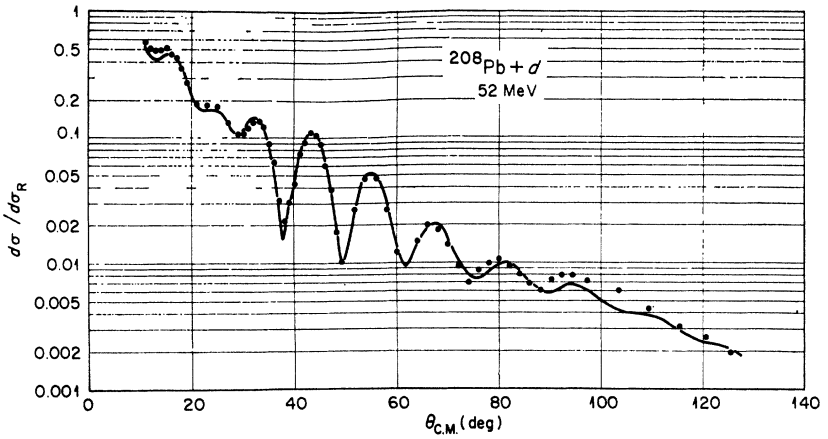

FIG. 6. Comparison with the data (Ref. 24) of the optical-model predictions for 52-MeV deuteron scattering from ^{208}Pb. The parameters of Table II were used.

tentials.[13] To lowest order we would expect the two potentials to be the same. However, comparison of the elastic scattering of the two particles, and also study of the (^{3}He, t) reaction between analog states, shows[13] that their optical potential contains a term proportional to $\mathbf{t}\cdot\mathbf{T}/A$ (where t is the isospin of the projectile and T is that of the target nucleus) which, for elastic scattering, becomes proportional to $\pm(N-Z)/A$. This term is complex, with the imaginary part peaked at the surface. It is uncertainties in this imaginary part which produce the largest uncertainties in the (d, t) calculations.

The form previously used[13] for the shape of the imaginary part of the symmetry term was the derivative of the Woods-Saxon form used for the main absorptive potential. By equating this to the first term in a Taylor expansion in the radius of the imaginary potential, we can interpret the symmetry effect as a decrease in this radius for tritons compared to ^{3}He. The symmetry effect assumed for the real potential is much less critical; it was taken to be simply a change in well depth. Using the values $V_1=40$ MeV and $W_1=7$ MeV (in the notation of Ref. 13) and the ^{3}He potential 1 previously deduced, we are led to the values $V=160$ MeV and $r_0'=1.5$ F given in Table II for the triton potential. The other parameters are taken to be the same for both particles; in particular, it is assumed that the increase in a' found necessary to explain the ^{3}He scattering from Pb is also appropriate for tritons. The values of V_1 and W_1 used were obtained[13] for $A\sim60$–90 and a bombarding energy of 20–25 MeV. It is a major extrapolation to assume that they are still appropriate at 50 MeV and $A\sim200$. Nonetheless, they are the only guides that we have available.

F. Nucleon Bound State

It is assumed that the wave function of the nucleon before pickup is the appropriate eigenfunction for a Woods-Saxon well with spin-orbit coupling, with a binding energy equal to the separation energy for the transition. This is likely to be a good approximation for the transitions to "single-particle" states which are of interest here, since ^{208}Pb is reasonably well described as a closed-shell nucleus. Nonetheless, there remain ambiguities in the values to be used for the parameters of this well; indeed, one of the purposes of this experiment was to see if differences in the wells for neutrons and protons could be detected.

The potential well used is parametrized as in Eq. (1), except that the spin-orbit strength is expressed as λ times the Thomas value. This gives $V_s\approx(\lambda V/180.6)$ MeV, where V is the corresponding well depth which is adjusted to give the binding energy required. The basic parameters used (Table II) were taken from the results[30] of a fit to neutron hole and particle energies and to Coulomb stripping cross sections for Pb. The proton parameters were assumed to be similar, except that λ was reduced so as to give $V_s\approx5$ MeV. The values of V for the orbits of interest here are given in Table III; we see that $V_n=45.6\pm0.8$ MeV for the neutron states and $V_p=60.6\pm0.5$ MeV for the protons. Variations about these parameter values were also tried and will be discussed below. They include allowing the radius r_s and diffuseness a_s of the spin-orbit coupling term to differ from the r_0 and a of the central well. This has effects on the magnitudes of the tails of the wave functions for various l,j states which are important for determining their relative pickup cross sections.

As was discussed in Sec. V C, nonlocality corrections of the type given by Eq. (2) may be applied to bound-state wave functions also. For these, the value of the constant C is determined by the normalization condition and is greater than unity. Because of the other uncertainties found, the bound wave functions used in the calculations to be discussed below did *not* include this correction. Its effect may be estimated in a trivial fashion, since the distorted-wave cross sections are very closely proportional to the square of the magnitude

[30] M. Dost, W. R. Hering, and W. R. Smith, Nucl. Phys. **A93**, 357 (1967).

TABLE III. Well depths for neutrons and protons bound in ^{208}Pb with a binding energy of B, using potential parameters of Table II.

	Protons					Neutrons					
Orbit[a]	$3s_{1/2}$	$2d_{3/2}$	$2d_{5/2}$	$1h_{11/2}$	$1g_{7/2}$	$3p_{1/2}$	$3p_{3/2}$	$2f_{5/2}$	$2f_{7/2}$	$1h_{9/2}$	$1i_{13/2}$
$V(C)$ (MeV)	61.0	60.0	60.5	61.7	58.2	45.7	45.8	45.3	44.8	44.9	46.4
$V(I)$ (MeV)	61.0	60.4	60.3	60.6	···	45.7	45.8	45.5	44.7	46.8	44.7
B(MeV)	8.02	8.37	9.69	9.36	11.50	7.39	8.28	7.96	9.73	10.82	9.02

[a] $V(C)$ is obtained with the use of constrained spin-orbit coupling ($r_s=r_0$, $a_s=a$), and $V(I)$ with independent spin-orbit parameters $r_s=1.10$ F, $a_s=0.50$ F.

of the tail of the bound-state wave function. The correction (2) increases this magnitude by the factor C and the predicted cross sections by C^2, and hence reduces the extracted spectroscopic factors by C^{-2}.

VI. ANALYSIS OF PICKUP DATA

The first calculations to be described used the potential parameters given in Table II to generate the wave functions for the picked-up neutron or proton. We thus delay any discussion of possible differences in these parameters for the two types of nucleon until other ambiguities in the analysis have been investigated.

A. (d, ^{3}He) Reaction

The angular distributions obtained from the distorted-wave calculations using the local, zero-range approximations are compared to the data for the $3s_{1/2}$ and $2d_{3/2}$ proton pickup transitions in Fig. 7. When no radial cutoff is used (i.e., when the contributions from the nuclear interior are included), there are striking discrepancies between experiment and theory. In particular, the $s_{1/2}$ angular distribution is predicted to have sharp and deep minima which are not seen in the measurements, and a peak is observed near 30° at the position of a theoretical minimum. Similar features, although not so marked, are seen for the $d_{3/2}$ distribution. The $d_{5/2}$ distributions, not shown in Fig. 7, are very much like those for $d_{3/2}$ pickup. The theoretical distribution for $h_{11/2}$ pickup also shows rather too much structure and falls off too slowly for angles less than 18°, and the $g_{7/2}$ shape is poor around 20°.

Calculations were also made including the effects of spin-orbit coupling in the distorted waves. This produced small changes for the $s_{1/2}$ transition, but the effects were negligible for $d_{3/2}$ and $d_{5/2}$.

Because the angular distributions are poorly reproduced, it is difficult to extract spectroscopic factors with any accuracy. Tentative values are included in Table IV, and it is seen they are approximately twice as large as the $2j+1$ expected.

1. Damping the Nuclear Interior

Corrections for the nonlocality of the distorting optical potentials were introduced by using Eq. (2) with just the real parts of the potentials and assuming that $\beta_d=0.54$ F and $\beta_3=0.3$ F, together with the analogous finite-range correction[21] for a range of 1.54 F. The result was mainly an over-all reduction in cross section by about 30%. The $l=0$ and $l=2$ distributions changed very little in shape, except for some filling of the $l=0$ minimum near 30°. The distribution for $h_{11/2}$ shows an increased slope on both sides of the main peak. The spectroscopic factors are now correspondingly increased by about 30%.

As mentioned earlier, improvement in the fits to (p, d) angular distributions has been obtained by further damping the contributions from the nuclear interior.[28] The ansatz adopted was to continue using the form (2) but arbitrarily to increase the β values. The most obvious signature of the changes produced here is the effect on the $s_{1/2}$ angular distribution near 30°. Increasing both the β values by a factor of 4 produces an additional peak here which resembles that observed, although a factor of about 6 is required for a good fit. This latter corresponds to eliminating almost entirely the contributions from the nuclear interior; even those from $r\approx 9.5$ F are damped by 50%. This damping also improves the fits to the measurements for $d_{3/2}$ and $d_{5/2}$, especially between 30° and 50°.

The magnitudes of the cross sections predicted are now reduced to about one-half those previously obtained, so that the spectroscopic factors required are now about *four* times the values $(2j+1)$ which are expected. This can be understood because it is clear the major contributions to the reaction (see discussion below and in Appendix B) come from the nuclear surface region and outside it. The rounded damping factors of Eq. (2) have tails which extend out to this region, so that in the process of eliminating the small contributions from the interior we also severely damp these major contributions outside. This leads us to turn, reluctantly, to the use of a sharp radial cutoff which is equivalent to a damping factor which is zero for radii less than some cutoff radius R_{co} and unity beyond it. We say "reluctantly" because clearly a *sharp* cutoff is unphysical. Nonetheless, it involves only one parameter, whereas any rounded generalization needs at least two. Certainly there is no physical justification for using the Eq. (2) when we depart so radically from the simple model upon which it is based.

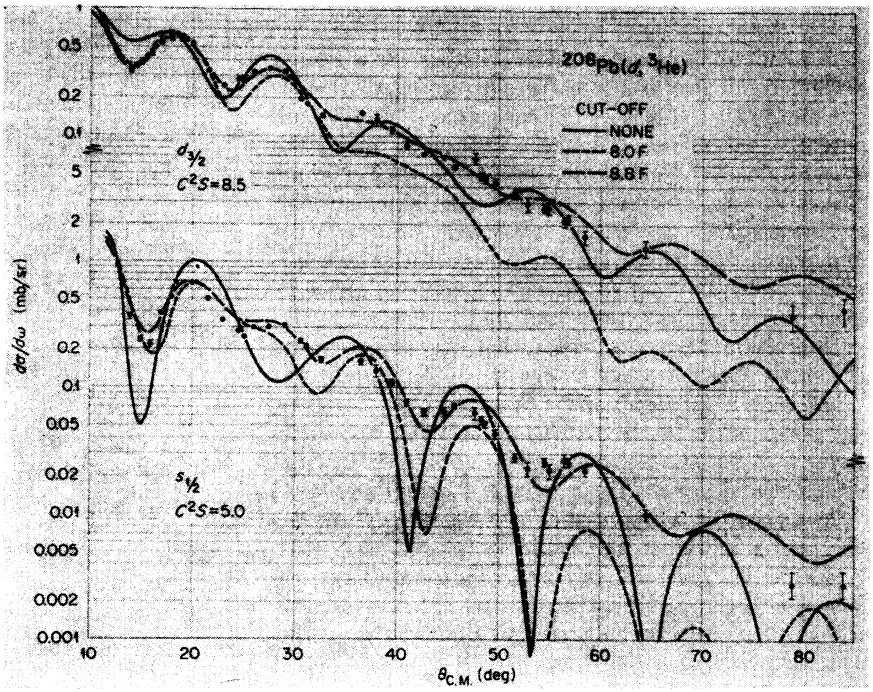

FIG. 7. Effects of a radial cutoff on the cross sections predicted by the distorted-wave theory and comparison with the measurements for proton pickup.

2. *Radial Cutoffs*

Figure 7 includes curves, still calculated with the local, zero-range approximations, but with sharp radial cutoffs of $R_{co}=8.0$ and 8.8 F. These are drawn using the same spectroscopic factors as for the cases with no cutoff. Clearly there is no drastic change in cross-section magnitudes associated with cutoffs in this range; indeed, not until the cutoff exceeds 9 F does the cross section begin to fall noticeably (see Appendix B). The angular distribution shapes are modified, however, especially for $s_{1/2}$ pickup. These modifications are not large until $R_{co}\gtrsim 8$ F, and the curve for $R_{co}=8.8$ F is seen to give a good fit to the data. (For orientation, we note that $8.8=1.43\ A^{1/3}$, so that this value of R_{co} is appreciably larger than the radius of the proton potential well or the radii of the real parts of the optical potentials. It is midway between the radii of the two absorptive potentials.) This choice for R_{co} also gives a good account of the angular distributions for the other transitions, as Fig. 5 shows. Many values of the cutoff radius were studied. Those of less than 8.8 F lead to angular distributions whose slopes are too steep for large angles, and values greater than this give too gentle slopes, so that the choice of optimum radius is quite well determined and appears to be approximately the same for all four transitions. The spectroscopic factors associated with the curves drawn in Fig. 5 are given in Table IV; they are approximately twice as large as the expected values of $2j+1$.

TABLE IV. Spectroscopic factors C^2S for the $(d, {}^3He)$ reactions obtained when the parameters of Table II and III are used.

	No cutoff[a]		Cutoff 8.8 F		
Orbit	CSO	ISO	CSO	ISO	$2j+1$
$3s_{1/2}$	(4)	(4)	4.5	4.5	2
$2d_{3/2}$	(8)	(8)	8.5	7.7	4
$2d_{5/2}$	(10)	(10)	10.0	10.7	6
$1h_{11/2}$	14	15	20.0	22.6	12
$1g_{7/2}$	(4)	...	5.6	...	8

[a] CSO means constrained spin-orbit coupling; ISO means independent spin-orbit parameters for the proton well. The values in parentheses are not well determined.

TABLE V. Changes in spectroscopic factors for $(d, {}^3He)$ reactions due to changes in the proton potential parameters. Radial cutoff at 8.8 F used.

		$3s_{1/2}$		$1h_{11/2}$	
r_0 (F)	a (F)	S[a]	V_p (MeV)	S[a]	V_p (MeV)
1.25	0.63	*1.0*	61.0	*1.0*	61.7
1.20	0.63	1.7	63.8	1.9	65.0
1.30	0.63	0.6	58.5	0.5	58.8
1.30	0.50	0.8	57.8	0.6	57.1
1.30	0.75	0.5	59.0	0.4	60.3
1.20	0.75	1.2	64.5	1.5	66.8
1.25	0.63[b]	1.0	61.0	1.1	60.6

[a] Normalized to unity for the first, standard set of parameters (Table II).
[b] With independent spin-orbit parameters $r_s=1.10$ F, $a_s=0.50$ F.

3. Optical-Potential Variations

It is now important to know whether these results are independent of other features of the calculations—specifically, the choice of optical-potential and proton potential parameters. First, the diffuseness a' for the ^{3}He imaginary potential was set at the smaller value of 0.81 F, which seems appropriate for lighter nuclei,[10] but which does not fit the observed ^{3}He scattering from Pb at 47.5 MeV. The only effect of this is a uniform increase in cross sections (and hence decrease in spectroscopic factors) of about 14%, which may be attributed to the weaker absorption that this value of a' implies. On the other hand, the optimum ^{3}He potential parameter sets 4 and 5 of Table I imply *greater* absorption of the ^{3}He waves and indeed yield distorted-wave cross sections which are about 20% smaller without any significant change in angular distribution shape.

The distorted-wave predictions were found to be even less sensitive to the deuteron potential, so that it appears that the need for a cutoff (or some equivalent device) is not removed by considering optical-potential ambiguities, provided that one maintains a fit to the observed elastic scattering data.

4. Variations in Bound-State Parameters

It now remains to consider variations of the proton potential parameters. Unfortunately, we have no independent way of determining these for the last few occupied shells in the way we do for the scattering problem. Only the tails of the bound-proton wave functions are important, and the *form* of these is determined by their binding energy. Hence we only expect the cross-section magnitudes to change when we vary the bound-state parameters, but not the angular distributions. This is indeed the case. Further, changes in the spin-orbit coupling strength should only affect the relative cross sections for $j=l\pm\frac{1}{2}$, but leave their average approximately unchanged. It was found, for example, that increasing the value of λ_p from 15 to the value 27.5 used for the neutrons (corresponding to the large value $V_{sp}\approx 9.5$ MeV) reduced the cross section for $d_{3/2}$ by about 6% and increased those for $d_{5/2}$ and $h_{11/2}$ by about 10 and 15%, respectively.

More dramatic changes are wrought by changing the radius r_0 or diffuseness a, as is shown by the examples given in Table V for $s_{1/2}$ and $h_{11/2}$ pickup. These changes in cross section are found to be very closely the same as the changes in the square of the tail of the wave function. (We return to another aspect of this result in Appendix A.) It seems necessary to increase either or both of these parameters considerably in order to reduce the spectroscopic factor for $s_{1/2}$ pickup to the value 2 expected for a closed shell. For example, $r_0\approx 1.30$ F and $a\approx 0.75$ F would give S close to 2 for $s_{1/2}$ and $S\approx 9$ for $h_{11/2}$.

Polarization measurements for the scattering of protons have shown that the spin-orbit coupling term is peaked inside the main central potential. This may be achieved by using a radius parameter r_s or diffuseness a_s, or both, which have smaller values than those for the central potential. Cross sections were computed using this "independent" spin-orbit term with $r_s=1.10$ F and $a_s=0.50$ F and the remaining parameters as in Table II. Again angular distributions are not affected, but the new spectroscopic factors required are included in Table IV. The changes are of order 10%, being positive for $j=l+\frac{1}{2}$ and negative for $j=l-\frac{1}{2}$. This brings the $d_{5/2}$ to $d_{3/2}$ *ratio* closer to the closed-shell value of 1.5.

B. (d, t) Reaction

The calculational procedure followed was similar to that for the $(d, ^3\text{He})$ reaction. Figure 4 compares the results of the distorted-wave predictions in the local, zero-range approximation without a radial cutoff and with one at 8.4 F, and using the optical potentials given in Table II. The corresponding spectroscopic factors C^2S are given in Table VI, and, except for the rather low value for $i_{13/2}$, are in good agreement with the values of $(44/45)(2j+1)$ expected[31] for a closed shell.

1. Interior Contributions

In contrast to the $(d, ^3\text{He})$ results, we see that the calculations without a cutoff give reasonably good fits to the observed angular distributions. The predictions for many different cutoff radii in the vicinity of the nuclear surface were studied, and the optimum value is around 8.4 F. It is definitely less than the optimum value of 8.8 F required for the ^{3}He transitions, and this is probably associated with the smaller radius used for the triton absorptive potential. However, this "optimum" value is not very well defined, since any such cutoff does not give better fits to the angular distributions than does no cutoff at all (except for the $i_{13/2}$ pickup, where the correct slope beyond the main peak is given by a cutoff close to 8.4 F but not without it).

Just as for the $(d, ^3\text{He})$ case, the effects of a rounded damping factor were also studied by using the form of Eq. (2) with arbitrarily increased nonlocalities. The results were very similar. A large degree of damping produces the same changes in the angular distributions as a radial cutoff near 8.4 F, but a reduction in cross sections (and hence an increase in spectroscopic factors) of about a factor of 2.

Using Eq. (2) with the more conventional values $\beta_d=0.54$ F and $\beta_t=0.3$ F (but ignoring any effect for the bound state), together with the analogous correction[21] for a finite range[22] of 1.69 F, gives about 10% decrease in all the cross sections. There are negligible changes in the angular distribution shapes at the forward angles, but a small increase in slope at the larger

[31] J. B. French and M. H. Macfarlane, Nucl. Phys. **26**, 168 (1961).

TABLE VI. Spectroscopic factors C^2S for the (d, t) reactions obtained when the parameters of Tables II and III are used.

	No cutoff[a]			Cutoff 8.4 F			
Orbit	CSO	ISO	^{3}He pot.	CSO	ISO	^{3}He pot.	$2j+1$
$3p_{1/2}$	2.0	1.9	2.7	2.0	1.9	2.7	2
$3p_{3/2}$	3.4	3.5	4.9	3.4	3.5	4.9	4
$2f_{5/2}$	6.0	4.9	8.9	6.0	5.0	9.2	6
$2f_{7/2}$	6.0	6.9	8.8	6.0	6.8	9.1	8
$1h_{9/2}$	9.0	7.4	16.8	9.0	7.3	16.5	10
$1i_{13/2}$	10.0	12.9	18.4	10.0	12.9	18.1	14

[a] CSO means constrained spin-orbit coupling; ISO means independent spin-orbit parameters for the neutron well. Column labeled "^{3}He pot." was obtained (with CSO) assuming that the triton potential was the same as for the ^{3}He (Table II).

angles. If Eq. (2) were applied to the bound states also (with $\beta_n=0.85$ F, say), this decrease in cross section would be changed into an increase of about 20%.

2. Optical-Potential Variations

Because there is considerable uncertainty in the relationship that was used to obtain the triton optical potential from the ^{3}He potential, calculations were also made assuming that these two potentials were the same. Thus we used $r_0'=1.6$ F and $V=175$ MeV instead of the values given in Table II. This produces small changes in the angular distributions, but no improvement except for the $i_{13/2}$ transition for which the slope at large angles is now given correctly without the use of a cutoff. The increased absorption associated with this potential, however, leads to the cross-section magnitudes being severely reduced, just as has been observed for lower deuteron energies.[8] As the values of the spectroscopic factors in Table VI show, these are then increased by amounts of between 40 ($l=1$) and 85% ($l=5$ and 6). While their *relative* values are now more closely proportional to $2j+1$, their absolute values have become too large. Further, if a radial cutoff near the nuclear surface is demanded, the optimum radius is now increased to a value closer to the 8.8 F found for the $(d, ^3\text{He})$ reaction.

3. Variations in Bound-State Parameters

The effects of using independent spin-orbit parameters $r_s=1.10\neq r_0$ and $a_s=0.50\neq a$ for the bound neutron were found to be similar to those described above for the proton pickup. There are no changes in the angular distributions, but the $j=l+\frac{1}{2}$ spectroscopic factors required are increased and those for $j=l-\frac{1}{2}$ are decreased. Their values are included in Table VI. This j-dependent action is important. As Table VI shows, with constrained spin-orbit parameters ($r_s=r_0$, $a_s=a$) the $f_{5/2}$ and $f_{7/2}$ S values are approximately the same, while those for $p_{3/2}$ and $p_{1/2}$ are in the ratio 1.7:1. The closed-shell values of $2j+1$ would give ratios of 1.33:1 and 2:1, respectively. Using the smaller r_s and a_s gives experimental ratios of about 1.4 and 1.8, so that the $l=3$ discrepancy is entirely removed. Further, the S for $i_{13/2}$ is now nearly equal to $2j+1$, whereas that for $h_{9/2}$ is reduced to only $\frac{3}{4}$ that value.

Varying the radius r_0 and diffuseness a of the neutron central potential again does not change the angular distribution, but modifies the magnitudes of the cross sections in a way almost exactly proportional to the square of the tail of the neutron wave function. The results of these calculations are summarized in Table VII for the $l=1$ and $l=6$ pickup; they show the same general features as were seen for proton pickup (Table V)—in particular, that the high l states are more sensitive to these parameter changes. For example, decreasing the radius to $r_0=1.20$ F and increasing the diffuseness to $a=0.75$ F leaves the S for the $p_{1/2}$ and $p_{3/2}$ transitions almost unchanged, but increases the S for $i_{13/2}$ to about 13.3, which is close to $2j+1$ for this state. However, this is with constrained spin-orbit coupling; using the independent spin-orbit parameters would then further increase the S for $i_{13/2}$ so that it became too large.

4. j Dependence for $l=1$ Transitions

The ratios of the observed cross sections for $p_{3/2}$ and $p_{1/2}$ pickup are plotted in Fig. 8 and show strong oscillations with angle. In the absence of spin-orbit coupling for the deuterons and tritons, the distorted-wave calculations for these transitions only differ in the slight change in the Q value required. The effect of spin-orbit coupling on the neutron wave functions only manifests itself as a small change in cross-section magnitude; for the parameters used here, the $p_{3/2}$ cross section is about 10% larger than that for $p_{1/2}$ due to this effect. Further, the ratio of these two cross sections is almost independent of angle. Including spin-orbit effects into the distorted waves, however, introduces the strong oscillations shown in the upper part of Fig. 8. The use of a cutoff gives a poorer fit to the data, whereas without a cutoff the agreement is very good both in shape and in magnitude. These curves were

TABLE VII. Changes in spectroscopic factors for (d, t) reactions due to changes in the neutron potential parameters. Normalized to unity for first, standard set of parameters (Table II). CO means radial cutoff.

r_0 (F)	a (F)	$3p_{1/2}$ V_n (MeV)	S No CO	S CO 8.4	$3p_{3/2}$ V_n (MeV)	S No CO	S CO 8.4	$1i_{13/2}$ V_n (MeV)	S No CO	S CO 8.4
1.25	0.63	45.7	*1.00*	*1.00*	45.8	*1.00*	*1.00*	46.4	*1.00*	*1.00*
1.30	0.63	43.0	0.76	0.72	43.2	0.76	0.74	43.7	0.62	0.62
1.25	0.75	45.7	0.78	0.73	45.8	0.80	0.76	47.7	0.83	0.83
1.20	0.75	48.7	1.02	0.96	48.7	0.96	1.01	50.8	1.33	1.33
1.25	0.63[a]	45.7	0.95	0.95	45.8	1.03	1.03	44.7	1.29	1.29

[a] With independent spin-orbit parameter $r_s = 1.10$.

drawn assuming that the ratio of spectroscopic factors was the same (1.7) as those given in Table VI and used in Fig. 4.

It was then of interest to see which channel was responsible for this effect. The lower half of Fig. 8 shows results (for a spectroscopic factor ratio of 2.0) for which only the deuteron, or only the triton, spin-orbit term was used. (The results for no cutoff are similar.) Switching off the spin-orbit coupling for both channels gives ratios essentially the same as those for the use of the triton term alone. Clearly it is the deuteron spin-orbit coupling which is responsible for the j dependence of the cross sections, in agreement with findings at a lower energy and for lighter nuclei.[32]

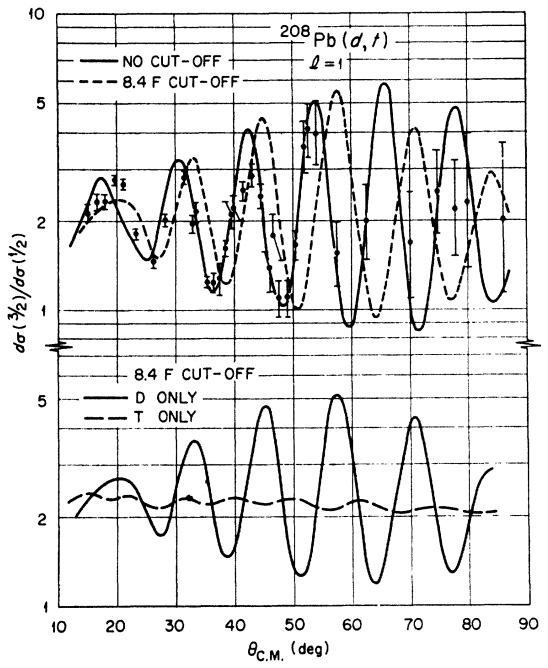

FIG. 8. The j dependence for $l=1$ neutron pickup showing the ratio of the cross sections for $p_{3/2}$ and $p_{1/2}$. The theoretical curves are described in the text; those in the upper half are drawn for $S(p_{3/2})/S(p_{1/2}) = 1.7$; those in the lower half assume 2.0 for this ratio.

This cross-section j dependence is associated with strong polarization effects. The left-right asymmetries produced by using 100% vector-polarized deuterons are predicted to be as high as 85% at the forward angles of 8°, 18°, and 33° for $p_{1/2}$ pickup and roughly half those values (but of opposite sign) for $p_{3/2}$ pickup. This suggests that measurement of these asymmetries could be a valuable spectroscopic tool for determining j values, just as in (d, p) reactions.[33] The asymmetries produced by tensor-polarized deuterons are much smaller at the forward angles but become larger as the angle increases. The polarization of the tritons produced by unpolarized deuterons is also smaller, being roughly $\frac{1}{3}$ the asymmetry due to vector-polarized deuterons.

VII. DISCUSSION OF THE ANALYSIS

A. "Model-Independent" Results

By this we mean results which only depend upon the theoretical analysis in a gross way or whose dependence is believed to be well understood. Among these we may count the identification of the transfer l value. This is clear in the case of the (d, t) reactions, but difficulties with the $(d, {}^3\mathrm{He})$ angular distributions make the identification of the l value somewhat ambiguous except for the $l=5$ pickup. One must accept the need for a radial cutoff before obtaining clear identification for $l=0$ and $l=2$.

Another such quantity is the ratio of cross sections for $j=l\pm\frac{1}{2}$ doublets. The $l=2$ pair for proton pickup from a closed shell would have spectroscopic factors with the ratio of $\frac{3}{2}$; experimentally this ratio depends upon the form of spin-orbit coupling assumed for the bound protons (Table IV). The independent form is

[32] B. M. Preedom, E. Newman, and J. C. Hiebert, Phys. Letters **22**, 657 (1966).

[33] T. J. Yule and W. Haeberli, Phys. Rev. Letters **19**, 756 (1967).

believed to be more realistic and gives a ratio of about 1.4, close to that expected.

Two doublets are excited by neutron pickup. That for $l=1$ shows spectroscopic factors (Table VI) in a ratio slightly less than the value 2 expected for a closed shell. The ratio of $2j+1$ values for $l=3$ is $\frac{4}{3}$. Again the independent form of neutron spin-orbit coupling gives spectroscopic factors which are in ratio close to this, whereas the constrained form would imply equal S values.

The other calculations made indicate that these j-dependent ratios are largely independent of the various uncertainties in the analysis, and could be deduced almost directly from the data. The distorted-wave calculations play a minor role in estimating the small corrections due to changes in Q value, and in reassuring us that the cross section is closely proportional to the square of the tail of the wave function for the picked-up nucleon.

B. Comparison of Neutron and Proton Pickup

We have seen that requiring good fits to the measured angular distributions leads to some difference between the two reactions. There is then a clear need to eliminate the contributions from the nuclear interior to the $(d, ^3\text{He})$ transitions, whereas this action leads to somewhat poorer agreement with the (d, t) measurements. Until this feature is better understood, it introduces an unpleasant note of uncertainty into any comparison of the spectroscopic factors obtained from the two reactions.

The spectroscopic factors C^2S obtained for neutron pickup are roughly in accord with the values $(44/45)(2j+1)$ expected[31] if ^{208}Pb were a closed-shell nucleus, but those for proton pickup are roughly twice these values. This discrepancy appears with or without the use of a radial cutoff. Further, it seems unlikely to be due to uncertainties in the ^{3}He optical potential, provided that this is chosen to be in agreement with the elastic scattering data. [Indeed, if we continue to use the same prescription for the triton potential, so that its parameters (especially r_0') bear a fixed relation to those for the ^{3}He potential, the *ratios* of the spectroscopic factors for neutron and proton pickup become largely independent of uncertainties in the ^{3}He parameters.]

It is natural to suppose that the discrepancy is indicating a need for a stretching of the proton wave functions by increasing the radius or diffuseness, or both, of the proton potential well relative to those for the neutron. For example, increasing the radius to $r_0 \approx 1.30$ F removes most of the discrepancy. However, in view of the other uncertainties, it was deemed premature to attempt to find an optimum set of values for the proton parameters. Not least among these uncertainties is our ignorance as to how close the spectroscopic factors should be to the closed-shell values of $2j+1$ (for protons) or $(44/45)(2j+1)$ (for neutrons).

Finding the expected values for the neutron spectroscopic factors may be taken as evidence supporting our prescription for obtaining the triton optical potential from the ^{3}He potential. On the other hand, while the difference that we have assumed between them is undoubtedly of the correct order of magnitude,[13] its precise value is much less certain. If, for example, we have overestimated the reduction in absorption appropriate for the tritons, then the neutron S values would have to be increased. Equating the two potentials would seem to give an upper limit to this uncertainty, and the results of Table VI indicate that the neutron S values would then be between 30 and 70% too large when independent spin-orbit parameters were used. If this limiting case were true, we would deduce that the neutron potential radius and/or diffuseness had to be increased also, although probably to a smaller extent than for the protons, so that even in this limiting case there remains some indication that the proton potential has a slightly greater radial extension than the neutron potential.

The "standard" set of neutron and proton potential parameters (Table II) was based upon the results of an analysis[30] of Coulomb stripping on ^{208}Pb. Comparison with the present work is legitimate because we have seen that the magnitudes of the pickup cross sections discussed here are also determined by the tails of the wave functions of the bound nucleons. That work was performed using a neutron potential with a constrained spin-orbit term. We may deduce from our results that the Coulomb stripping spectroscopic factors of Ref. 30 for $2g_{9/2}$ and $1i_{11/2}$ neutron capture would be much closer to unity if an independent spin-orbit term were used together with the neutron well parameters of Table II, although a small increase in r_0 could not be ruled out. The S value for $j_{15/2}$ neutron capture would then be increased even further above the expected value of unity. However, this state in ^{209}Pb is known to have an enhanced γ decay rate[34] which implies some mixing of the collective 3^- core excitation coupled to, say, the $g_{9/2}$ orbit; this would reduce its spectroscopic factor *below* unity. In the Coulomb stripping experiment this state had a very small cross section, so that it is conceivable that a second-order core-excitation process[35] could contribute significantly and account for the apparent large S value. The excitation of this state with deuterons of higher energy[8] shows relatively much larger cross sections and also more reasonable spectroscopic factors.

Hence, despite the various uncertainties which have been discussed in somewhat exhaustive detail, an over-all picture begins to emerge from the present analysis. It seems likely that neutron potential pa-

[34] C. Ellegaard, J. Kantele, and P. Vedelsby, Phys. Letters **25B**, 512 (1967).

[35] S. K. Penny and G. R. Satchler, Nucl. Phys. **53**, 145 (1964); B. Koslowsky and A. de Shalit, *ibid.* **77**, 215 (1966); P. J. Iano and N. Austern, Phys. Rev. **151**, 853 (1966).

TABLE VIII. Spectroscopic factors for ^{208}Pb (^{3}He, d) reactions[a] obtained when parameters of Table II are used. CSO means constrained spin-orbit parameters; ISO means independent spin-orbit parameters for the proton well. Radial cutoff at 8.8 F used. R is $2j+1$ times the proton spectroscopic factor divided by the corresponding neutron spectroscopic factor from Table VI.

		$3p_{3/2}$	$2f_{5/2}$	$2f_{7/2}$	$1h_{9/2}$	$1i_{13/2}$
CSO	C^2S	1.22	1.60	1.41	1.45	1.03
	R	1.44	1.60	1.88	1.61	1.45
ISO	C^2S	1.23	1.38	1.52	1.23	1.19
	R	1.41	1.66	1.79	1.68	1.29

[a] Reference 36.

rameters close to those in Table II give a reasonable account both of the present neutron pickup data and of the Coulomb stripping measurements. It seems necessary, however, to increase the spatial extent of the proton wave functions by increasing either the radius or the diffuseness, or both, of this potential. In other words, a reasonable interpretation of the present measurements leads to a larger spatial extension for the protons than for the neutrons, in the last filled major shell.

VIII. COMPARISON WITH SIMILAR MEASUREMENTS

A. ^{208}Pb(d, t) Reaction

Neutron pickup from ^{208}Pb via the (d, t) reaction has also been measured[8] at 15, 20, and 25 MeV. The distorted-wave analysis[8] of those results employed potential parameters which were somewhat different from those used here. Spectroscopic factors similar to those in Table VI were obtained (using $r_0=1.225$ F, $a=0.70$ F, and a constrained spin-orbit term with $\lambda=25$ for the neutron well), except that those for $h_{9/2}$ and $i_{13/2}$ were larger than found here. However, a glance at Table VII shows that the use here of the same values for r_0 and a would yield S values for these two transitions in good agreement with the previous work. In particular, the lower-energy results also showed ratios of spectroscopic factors for the $j=l\pm\frac{1}{2}$ doublets in good agreement with those found here.

B. ^{208}Pb(^{3}He, d)^{209}Bi Reaction

Measurements on the excitation of single-particle states by this reaction have been made[36] with ^{3}He ions of 51.26-MeV energy. These are of interest because the energies involved are very close to those for the present experiment, and we may ask whether these data also require the use of a radial cutoff and whether, under similar conditions, they also yield spectroscopic factors which are too large.

Distorted-wave calculations were made using the same parameters as in Table II, both with and without radial cutoffs. Unfortunately, the measured angular distributions only cover the angular range from 5° to 25°, and the effect of a cutoff is not very marked in this region. There certainly is no unambiguous case like that shown in Fig. 7 for $s_{1/2}$ pickup, although both the $h_{9/2}$ and $i_{13/2}$ stripping distributions for angles less than 15° are reproduced much better when a cutoff near 8.8 F is used. The fits to the $l=1$ and $l=3$ distributions are actually worsened a little by using a cutoff. Further, the original analysis[36] of these data was made using a ^{3}He potential similar to ours except that $a'=0.81$ F, as well as a slightly different deuteron potential. These gave quite good fits to the $h_{9/2}$ and $i_{13/2}$ distributions without the use of a cutoff.

It follows that we cannot obtain any conclusive supporting evidence for the need for a cutoff from these data. The spectroscopic factors that we obtain when normalizing to the peak value of the measured cross sections (and using a cutoff at 8.8 F) are given in Table VIII and range from 1.03 to 1.60. Using the independent spin-orbit parameters for the captured proton reduces the scatter in these values somewhat. Although they remain significantly greater than unity (indicating the need for a slightly larger radius or diffuseness for the proton well), the excess is not as large as the factor of 2 found for proton pickup.

These experimental results are also of interest because they involve protons in the same single-particle orbits as those from which the neutrons are picked up in the (d, t) reaction. Table VIII includes the ratios R of the proton spectroscopic factors to the neutron spectroscopic factors (divided by $2j+1$), obtained when the parameters of Tables II and III are used. These ratios are closely the same whether or not a cutoff is used. We see that the proton values are 44 to 88% larger than those for the neutrons. If we suppose that configuration-mixing effects would be about the same on the average for the neutron hole and proton particle states, these results imply again that the proton potential well should have a larger radius and/or diffuseness that the neutron well.

IX. POTENTIALS OF ROST

Parameters have been obtained by Rost[37] for shell-model potential wells of Woods-Saxon form which provide a best fit to the single-particle and single-hole energy levels in ^{208}Pb$\pm$1 nucleon nuclei. These potentials use independent spin-orbit (ISO) coupling and have $a=0.7$ F. That for protons has $r_0=1.275$ F, while that for neutrons has $r_0=1.347$ F. Distorted-wave calculations were made for the present experiments using these potentials for the picked-up nucleon. There are no significant changes in the shapes of the angular distributions, but the cross-section magnitudes are all increased.

[36] B. H. Wildenthal, B. M. Preedom, E. Newman, and M. R. Cates, Phys. Rev. Letters **19**, 960 (1967).

[37] E. Rost, Phys. Letters **26B**, 184 (1968).

The general results could be foreseen. We have already indicated that reasonable ($\sim 2j+1$) values for the (d, ^{3}He) spectroscopic factors would be obtained if the radius of the proton potential were increased from $r_0 = 1.25$ F to about $r_0 = 1.30$ F. Rost's potential has an intermediate radius, and results in cross sections which are between 1.1 and 1.7 times larger than with the parameters of Table II (the increase is j-dependent because of the ISO coupling in his potential). The proton spectroscopic factors are then all about $\frac{3}{2}$ times larger than the expected $2j+1$ values, so that a further increase in radius is still required.

We have already obtained reasonable ($\sim 2j+1$) values for the neutron spectroscopic factors when using the neutron potential of Table II with $r_0 = 1.25$ F. Clearly an increase of this to nearly 1.35 F will yield much too large cross sections (cf. Table VII). We find increases ranging from a factor of 2 (for $l=1$) to a factor of 3 ($l=5$ and 6), so that the corresponding spectroscopic factors now have $\frac{1}{2}$ or less of their expected values. The same criticism arises if we use these parameters in an analysis of Coulomb deuteron stripping[30] on ^{208}Pb. Indeed, the latter measurements, whose analysis is independent of optical-potential ambiguities, led to the choice of parameters given in Table II. The parameters of Rost would lead to comparable reductions in the spectroscopic factors in this case also. Again, their use in the interpretation of the lower-energy (d, t) measurements[8] would result in spectroscopic factors between 2 and 3 times smaller than $2j+1$.

We must conclude that Rost's neutron parameters are unacceptable in the present context if we believe that these states in ^{207,209}Pb are related to ^{208}Pb by the simple addition or removal of a neutron without appreciable rearrangement of the rest, i.e., that they are approximately "single-particle" states. That this is a reasonable belief is evidenced by the lack of fractionation of the transfer strength among other states. The proton potential of Rost, however, is much more acceptable, although a further small increase in radius seems to be required. Such an increase would not make his fit to the separation energies much worse. Of course, there is no *a priori* reason that potentials obtained in these quite different ways should be exactly the same.

It has been pointed out recently[38] that filling Rost's proton potential gives a proton density distribution for ^{208}Pb which is in good agreement with electron-scattering measurements. It was also shown that filling his neutron potential gives a neutron distribution whose rms radius is in striking agreement with that deduced recently[3] from proton scattering measurements. However, it has also been suggested recently[4] that the neutron rms radius may be appreciably smaller than the value deduced in Ref. 3.

[38] L. R. B. Elton, Phys. Letters **26B**, 689 (1968).

X. CONCLUSIONS

Two results from the analysis of the present experiment stand out most strongly:

(i) It is necessary to remove the contributions from the nuclear interior to the distorted-wave amplitudes in order to reproduce the observed (d, ^{3}He) angular distributions, whereas the agreement between calculated and measured distributions for the (d, t) reactions are generally not improved if this is done.

(ii) The spectroscopic factors for proton pickup are about twice as large as the expected values ($2j+1$) when we use for the proton potential the same radius and diffuseness parameters that in the neutron potential give reasonable spectroscopic factors for neutron pickup.

The apparent difficulty (ii) can be removed by allowing the proton wave functions to "expand," particularly by using a larger radius parameter for the proton potential well. The spectroscopic factors are also somewhat sensitive to uncertainties in the ^{3}He optical-potential parameters, but the result (ii) is *not* sensitive to the use or not of a radial cutoff. However, the result (i) is *not* dependent upon the choice of optical-potential parameters and until its origin is understood any conclusions drawn from result (ii) must be treated with some reservation.

When the results from the ^{208}Pb(^{3}He, d) reaction at similar energies are analyzed using the same parameters, we find slight but inconclusive support for the use of a radial cutoff in proton transfers. The spectroscopic factors obtained are also somewhat larger than unity, but the excess is not as great as for proton pickup. When the proton S values are compared to those for neutron pickup from the same orbits, we find ratios significantly greater than unity, which again seems to imply the need for a proton potential of greater spatial extent than that for neutrons.

These conclusions concerning the comparison of the neutron and proton potentials are based upon somewhat circumstantial evidence. However, most of the uncertainties are such that reasonable changes would either accentuate or not affect the conclusions. The major exception is our lack of understanding of the apparent need for a radial cutoff in the analysis of the (d, ^{3}He) reactions. Although the use or not of a cutoff does not *per se* affect the spectroscopic factors much, it may be symptomatic of some other difficulty. For example, the need to eliminate the interior may be due to neglect of damping of the distorted waves due to the nonlocality of the true optical potentials. If these nonlocal effects were associated with the *imaginary* part of the optical potentials, their spatial localization could be somewhat different for the two reactions because the most important difference between the triton and ^{3}He potentials appears to be in the spatial extent of their imaginary parts.

We have assumed that, to a first approximation, the

spectroscopic factors should have the values $(2j+1)$ appropriate for pickup from closed shells. We do expect some mixing, however, especially due to coupling to the octupole vibrational state of the ^{208}Pb "core." Such core-excitation effects have been observed[39] in ^{209}Bi. The single-hole state with spin j has admixed to it some of the 3^- core state together with the single-hole state j' coupled to a resultant j. Because of the odd parity of the core state, the j and j' orbits must be of opposite parity. (Of course, other core states may participate also, although the octupole coupling is expected to be the strongest.) As a consequence, the spectroscopic factor is reduced (the missing strength reappearing in the corresponding member of the core-excitation multiplet formed by coupling the 3^- state to the lowest single-particle state, etc.). If the amount of core admixture is estimated using the collective model and first-order perturbation theory and ignoring blocking effects, the angular momentum structure of the spin-independent interaction makes the amplitude of admixture much smaller when $j+j'$ is odd (requiring spin flip) than when it is even. Furthermore, the amplitude is proportional to $(2j'+1)^{1/2}$.

Of the proton hole states considered here, the $h_{11/2}$ may be mixed with $(3^-, d_{5/2})$, and correspondingly the $d_{5/2}$ may have admixed some $(3^-, h_{11/2})$, in an obvious notation. The proportionality to $2j'+1$ implies that the reduction in S for $d_{5/2}$ should be twice that for $h_{11/2}$. The $d_{3/2}$ and $s_{1/2}$ should be little affected because they require coupling to hole states in the next shell. Similarly, of the neutron hole states, only the $i_{13/2}$, $h_{9/2}$, and $f_{7/2}$ should be affected to lowest order. The coupling between $i_{13/2}$ and $h_{9/2}$ has $j+j'$ odd and is much weaker (by about a factor of 5) than between $i_{13/2}$ and $f_{7/2}$. For the latter pair, again the reduction in S for $f_{7/2}$ is predicted to be nearly twice that for $i_{13/2}$. There is, perhaps, some indication that these states have lower spectroscopic factors than the others, but apparently the effect is not large. It could be obscured by other uncertainties, especially by the j dependence of the effects of the spin-orbit coupling on the bound-nucleon wave functions.

The proton hole state at 3.48 MeV, assigned $g_{7/2}$ in Table IV, shows only $\frac{1}{3}$ to $\frac{1}{2}$ the pickup strength that would be expected relative to the other states. This, together with the fact that the well depth needed to give $1g_{7/2}$ proton state at this energy is less than for the other states, implies that most of the strength is to be found at higher excitation energies. The upper limit on the cross section for the $\frac{9}{2}^+$ level at 2.73 MeV in ^{207}Pb corresponds to $C^2S \lesssim 0.1$ and puts an upper limit of 5% on the intensity of admixture into the ^{208}Pb ground state of the ^{206}Pb core coupled to $(g_{9/2})^2$ neutrons.

ACKNOWLEDGMENTS

We are indebted to Claude Ellsworth for preparation of the target and for determining its thickness. We wish to thank the authors of Ref. 24 for making their data available in advance of publication. Dr. R. M. Drisko kindly made available the optical-model code HUNTER and distorted-wave code JULIE, and provided helpful advice. It is a pleasure to acknowledge the help and support of Dr. B. G. Harvey and the entire group of the 88-in. cyclotron. Three of us (W.C.P., H.H.D., and J.S.) would like to thank the Lawrence Radiation Laboratory, and particularly Dr. B. G. Harvey, for making the facilities of the laboratory available to them and their stay so pleasant.

APPENDIX A: REDUCED WIDTHS

Many uncertainties in the extraction of spectroscopic factors have been discussed. These fall into two categories. The first is concerned with uncertainties in the description of the reaction, principally through the optical-model parameters. The second is due to our lack of knowledge of the parameters for the bound-state wave functions; indeed, one purpose of the present work was to obtain information about these, assuming that the spectroscopic factors had essentially the closed-shell values of $2j+1$. However, the division into wave function times spectroscopic amplitude is a theoretical artifact; the measurements yield (to within the uncertainties of the first category) values for their product, namely, the form factor[40] or overlap of the wave functions for target and residual nuclei (see Appendix to Ref. 41, for example). In the distorted-wave calculations we use the single-particle model for the form factor

$$R_{lj}(r) = \vartheta_{lj} u_{nlj}(r), \tag{A1}$$

where u_{nlj} is a normalized eigenfunction for the $(n\,l\,j)$ orbit in a Woods-Saxon potential, and the corresponding spectroscopic factor is then $S=(2j+1)\vartheta_{lj}^2$. If we knew accurately that the potential parameters for $u_{nlj}(r)$ and the closed-shell assumption were correct, we would have $\vartheta_{lj}=1$. However, the one feature of which we are sure[40] is the *shape* of the tail of the form factor $R_{lj}(r)$ [namely, it is proportional to the Hankel (neutron) or Whittaker (proton) function corresponding to the known separation energy of the nucleon], and this is reproduced correctly by the model (A1). Now we have emphasized that the cross sections for the present experiment are, to a very good approximation, proportional to the square of the magnitude of this tail of the form factor. Hence we may extract from the experimental results values for $R_{lj}^2(r)$ at large r which are independent of the model used for the bound state, and in particular of the separation (A1). These may be expressed in terms of the dimensionless reduced widths[42]

$$\theta^2(lj) = \tfrac{1}{3} R_0^3 (2j+1) R_{lj}(r=R_0)^2. \tag{A2}$$

[39] C. Ellegaard and P. Vedelsby, Phys. Letters **26B**, 155 (1968).

[40] N. Austern, Phys. Rev. **136**, B1743 (1964); W. T. Pinkston and G. R. Satchler, Nucl. Phys. **72**, 641 (1965).

[41] K. K. Seth, J. A. Biggerstaff, P. D. Miller, and G. R. Satchler, Phys. Rev. **164**, 1450 (1967).

[42] J. B. French, in *Nuclear Spectroscopy*, edited by F. Ajzenberg-Selove (Academic Press Inc., New York, 1960), Pt. B

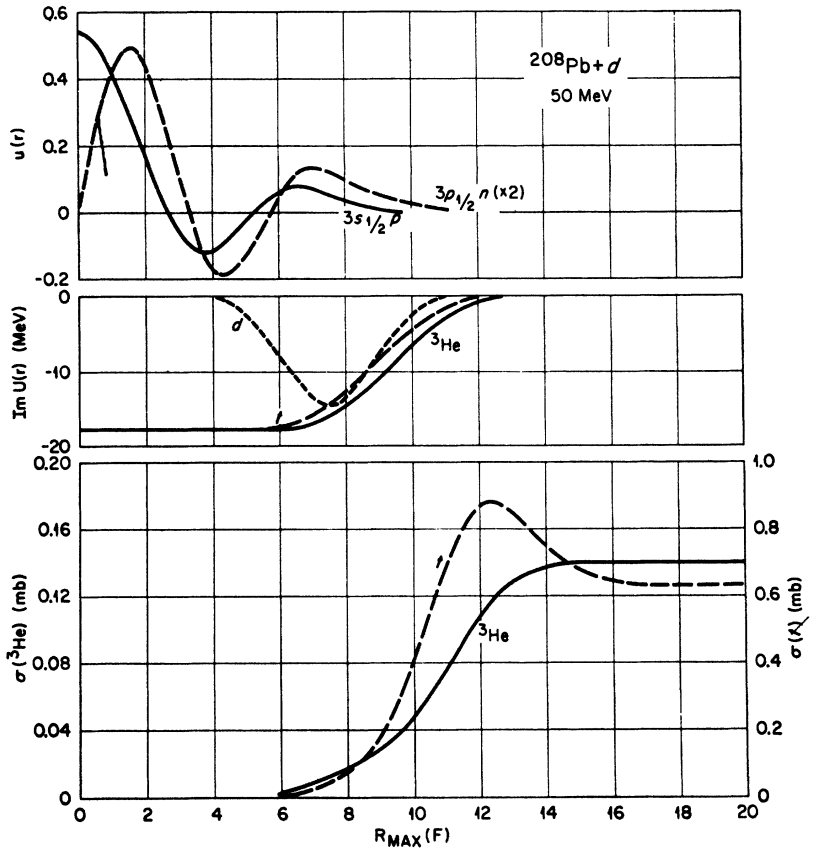

FIG. 9. Radial distribution of contributions to the pickup reactions (lowest curves), of the imaginary parts of the optical potentials (center curves), and of the wave functions of the picked-up nucleons (top curves).

Of course, these values still depend upon the choice of radius $r=R_0$. We could remove this dependence by choosing sufficiently large r and dividing out the appropriate Hankel or Whittaker function, but it is more convenient merely to quote the θ^2 themselves. Inspection shows that the form factors have assumed their asymptotic form for $r \gtrsim 10$ F, so that we choose $R_0=10$ F. Note that $10=1.68\ A^{1/3}$ here, and that the Woods-Saxon potential of Table II has fallen to a value of about -1 MeV at $r=10$ F. Values of θ^2 are given in Table IX for this radius; they correspond to the same theoretical cross sections as those for which spectroscopic factors are listed in Tables IV and VI (with the use of a cutoff) and which are shown in Figs. 4 and 5.

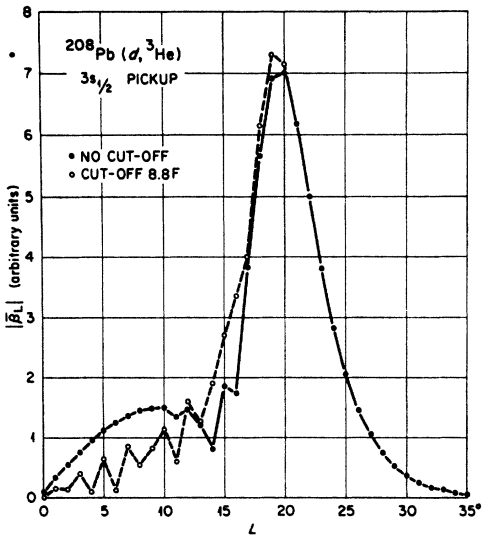

FIG. 10. Contributions from various partial waves to the amplitudes for pickup of a $3s_{1/2}$ proton from ^{208}Pb.

APPENDIX B: SOME PROPERTIES OF THE DISTORTED-WAVE AMPLITUDES

In a search for a better understanding of the results of using a radial cutoff on the distorted-wave integrals, these were studied in some detail. First, we show in Fig. 9 the regions which contribute importantly to the reaction. Plotted there is the integrated cross section

$$\sigma(R_{\max})=\int_0^{2\pi}\int_0^{\pi}\frac{d\sigma}{d\omega}\,d\omega \qquad \text{(B1)}$$

for $3s_{1/2}$ proton pickup and $3p_{1/2}$ neutron pickup as a function of the maximum radius, $r=R_{\max}$, to which the stripping integrals are carried. In both cases we see that there are negligible contributions from $r \lesssim 6$ F and that the major contributions come from quite large radii. For orientation we show to the same radial scale both the radial wave functions for the nucleon picked up and the absorptive parts of the optical potentials.

TABLE IX. Values of the reduced widths $\theta(lj)^2$ for neutron and proton pickup from ^{208}Pb evaluated at $R_0=10$ F. The isospin factor was assumed to be $C^2=1$ for neutrons and $C^2=45/46$ for protons.

	Neutron						Proton			
Orbit	$3p_{1/2}$	$3p_{3/2}$	$2f_{5/2}$	$2f_{7/2}$	$1h_{9/2}$	$1i_{13/2}$	$3s_{1/2}$	$2d_{3/2}$	$2d_{5/2}$	$1h_{11/2}$
Separation energy (MeV)	7.39	8.28	7.96	9.73	10.82	9.02	8.02	8.37	9.69	9.36
θ^2	0.130	0.205	0.177	0.174	0.0408	0.102	0.0319	0.0364	0.0429	0.0396

The latter show that the reaction is largely confined to the outer regions by the absorption of the complex particles, while the former explain vividly why the cross sections are proportional to the squares of the wave-function tails.

Although the contributions from $r<8.8$ F are small, we saw that in the $(d, {}^3\mathrm{He})$ reaction they had important effects on the angular distributions. Of course, it is not the cross sections from different radii but the amplitudes which are additive, and it is the interference between contributions from different radii which makes the angular distributions more sensitive to a radial cutoff. Figure 10 shows the magnitudes of the reaction amplitudes[20] $\bar{\beta}_L$ for various partial waves for $3s$ proton pickup, where the differential and integrated cross sections are given by

$$d\sigma/d\omega \propto |\sum_L \bar{\beta}_L P_L(\theta)|^2, \qquad \sigma \propto \sum_L |\bar{\beta}_L|^2/(2L+1).$$

(The real and imaginary parts of the $\bar{\beta}_L$ have a very similar behavior.) As expected for a surface reaction, they peak strongly for $L\approx 20$. The classical distance of closest approach R_c for an orbit with angular momentum L is given by

$$L=[kR_c(kR_c-2\eta)]^{1/2},$$

where k is the particle wave number and η is its Coulomb parameter. For $L=20$, $R_c=10.5$ F for the deuterons and $R_c=10.6$ F for the ^{3}He, so that there is perfect matching for an $l=0$ transfer near this radius. The FWHM of the $\bar{\beta}_L$ curve is $\Delta L\approx 7$, corresponding to a radial spread of about 3 F.

The use of a radial cutoff at 8.8 F only affects the partial-wave amplitudes for $L\lesssim 20$. Classically, $R_c=8.8$ corresponds here to $L=15.1$ (^{3}He) or 16.3 (d). Eliminating radii less than 8.8 F strongly reduces the $\bar{\beta}_L$ for small L, but enhances those for $L\approx 15$. It is this latter effect which improves the fit to the shape of the angular distribution for this reaction (see Fig. 7); as noted earlier, a cutoff at 8 F or greater is required to produce something resembling the measured shape near 30°. Note that the peak of the $\bar{\beta}_L$ curve obtained with a cutoff is more symmetrical, and in fact the improvement for $L\approx 15$ appears to be due to the absence of some destructive interference which is present for the case with no cutoff. Thus we are concerned with a small modification of the distorted-wave amplitudes which is quite well localized both radially and in angular momentum. The radial position is at a place where the absorption due to the optical potentials is large and certainly at a place where the "true" distorted waves may be appreciably different from those generated by the simple, local, optical potentials used here.

The structure of the corresponding partial-wave amplitudes for the (d, t) reaction is very similar to that shown in Fig. 10. (They are more complicated to display for $l\neq 0$ because there are more parts. For example, with transfer $l=1$, each incoming partial wave L_d is linked to two outgoing waves with $L_t=L_d\pm 1$, and there are amplitudes for the $m=0, \pm 1$ components of l.) They peak at an L_d value two or three units larger than for the $(d, {}^3\mathrm{He})$ reaction, with about the same peak width but a longer tail for large L. Here $L_d=22$ corresponds to the classical approach radius of $R_c=11.4$ F. The triton angular momentum for this radius is $L_t\approx 26.5$; the difference $|L_d-L_t|\approx 4.5$ is much larger than the transfer $l=1$ and implies appreciable momentum mismatching.[43] This does not appear to enhance the importance of the nuclear interior,[44] because the gain from the improved matching there is overwhelmed by the loss due to the absorption from the deuteron and triton distorted waves. Presumably, it is responsible for the more complicated structure of the $\sigma(R_{\max})$ curve (Fig. 9) for this reaction, and also results in the somewhat greater spread in L values from which important contributions come. In particular, there appears to be destructive interference by contributions from quite large radii ($r>12$ F).

The structure of the deuteron, triton, and ^{3}He distorted waves was also studied, but this provided no further clues. The deuteron wave shows a strong focus at $r\approx 6.2$ F along the axis on the dark side with a peak twice the magnitude (unity) of the external wave; elsewhere in the interior it is structureless, and is damped on the illuminated side to about $\frac{1}{3}$ the external magnitude. The ^{3}He and triton waves are much more strongly damped in the interior and both show a weak focus at $r\approx 4$ F. Aside from subsidiary diffraction maxima for the triton, these two waves are rather similar.

[43] N. Austern, Ann. Phys. (N.Y.) **15**, 299 (1961).
[44] R. Stock, R. Bock, P. David, H. H. Duhm, and T. Tamura, Nucl. Phys. **A104**, 136 (1967).

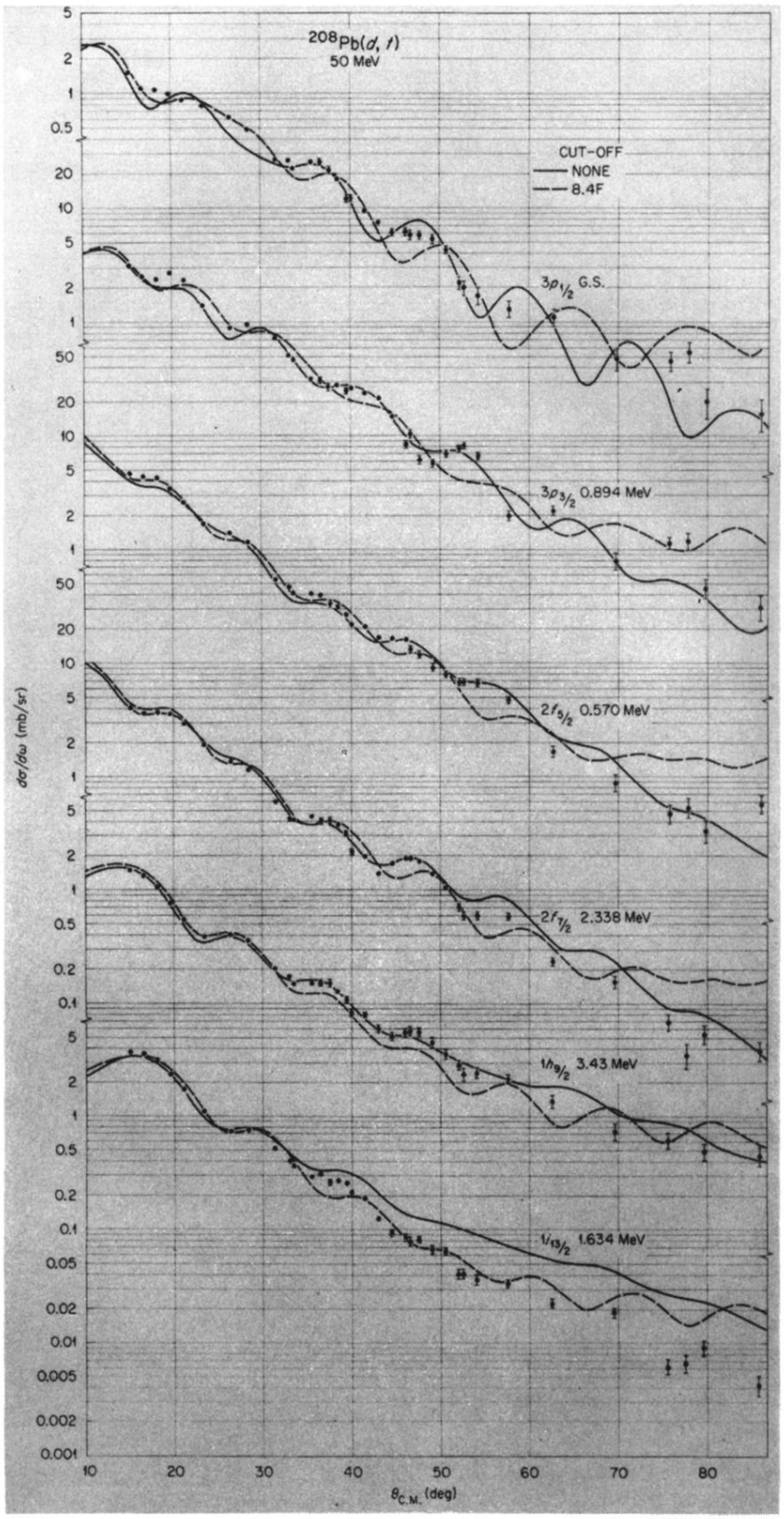

FIG. 4. Differential cross sections for neutron pickup by the ^{208}Pb$(d, t)^{207}$Pb reaction. The excitation energies and angular momenta are given for each group. The curves are distorted-wave predictions as described in the text.

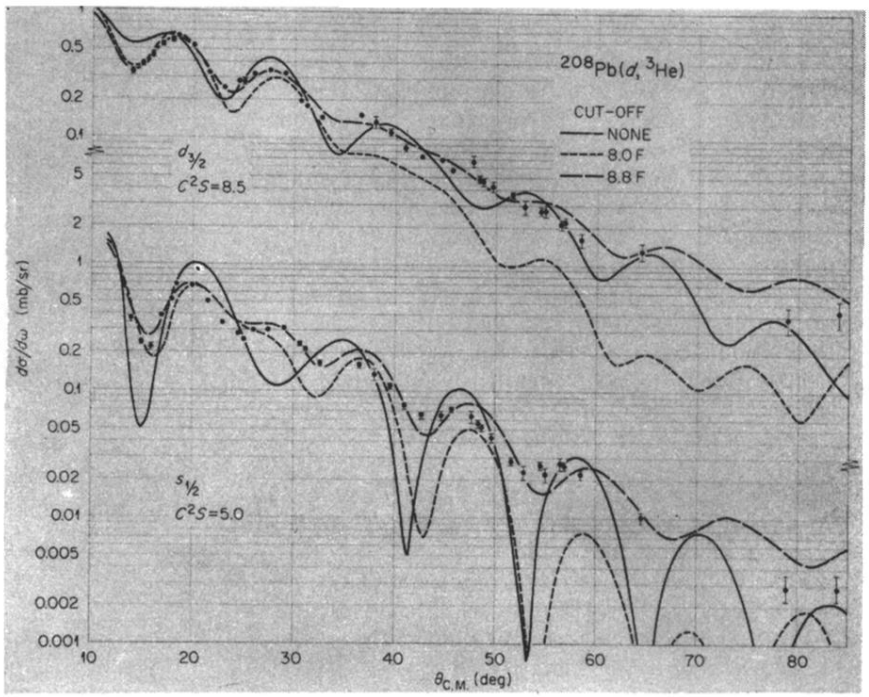

FIG. 7. Effects of a radial cutoff on the cross sections predicted by the distorted-wave theory and comparison with the measurements for proton pickup.